



**Analytic and Numerical Analysis of Cylindrical  
Corrugated Waveguide as a Promising Structure  
for Terahertz Applications**

By

**Warittha Suaingam**

*Supervisor*

Dr. Jonathan Gratus

A thesis presented for the degree of  
Master of Science by Research in Physics

Department of Physics  
Lancaster University

October 2024

---

## DECLARATION

I declare that this thesis, titled “Analytic and Numerical Analysis of Cylindrical Corrugated Waveguide As a Promising Structure for Terahertz Applications” is my own original work. The material has not previously been submitted at any university or for publication, either in its entirety or in part. This thesis does not exceed the maximum permitted word count of 35,000. The approximate word count of is 10,209.

Warittha Suaingam  
October, 2024

---

# Abstract

Terahertz radiation with its non-ionizing property can be potentially employed in many fields, for example, medical imaging, security scanning, spectroscopy, and communication. In this thesis, we investigate one of the potential terahertz generators based on the cylindrical corrugated waveguide.

We show that by applying the Mathieu equation in Maxwell's equations specifically for our symmetric corrugated waveguides, we can find the explicit approximate solution of the electromagnetic fields. Moreover, we define the coincident inflection point (CIP) which is the point on the dispersion relation where particles would interact with the broad frequencies range of the electric fields. With this approximation and the CIP, the design of the symmetric corrugated waveguides is easier compared to other slow-wave structures e.g., radio frequency cavity.

We utilize the CST studio to compare our analytical results with numerical results from the CST simulation. The results show good agreement in the longitudinal electric field graphs and the dispersion relation between these two results, confirming that our analytical results are good enough to use in practice.

The study in the cylindrical corrugated waveguide is the developed work from the rectangular corrugated waveguide. Not only did we observe better agreement between analytical results and numerical results, but also an easier in manufacturing process. We expect that the optical fiber extrusion technique for making the cylindrical corrugated structure will be relatively easier and cheaper than the CNC (Computer Numerical Control) technique for the rectangular corrugated structure.

---

## Acknowledgment

For one year that I have spent to do an MRes course at Lancaster University. I am very grateful for this opportunities to studying in the lovely place, meeting wonderful people, and gaining new experiences, all of these are my precious memory that will not forget.

I would like to express my deepest appreciation to my talented, brilliant, incredible, amazing, spectacular, intelligent, the one and only supervisor, Dr. Jonathan Gratus who give me an opportunity to work under his supervision. With his guidance and support in everything not only academic but also helping me to looking for societies and events that I could join and meet new people, I am able to complete this academic year with his support.

I could not have undertaken this journey without my college, Sergey Siaber who pertinently teaches me a lot of thing during my program such as running simulations of CST, giving a guidance about the theory in waveguides and gives me suggestion about the writing a thesis.

And I should not forget to thank you to both Jonathan and Sergey for giving me a supportive environment during our meetings, and helping me to name a title of this thesis. It was my pleasure working with these two excellent people.

I would like to extend my sincere thanks to Louise Innes who help me with my thesis writing. I am really appreciated new prospective of seeing things and advice that she gave me. Beside academic writing, I was very excited to spend time with her talking about movies and books.

Many thanks to Rebecca Seviour for helping with the CST simulation, Prof. Steven Jamison, and Prof. Helen O’Keeffe who are my deputy supervisor and my independent supervisor for helping to find my knowledge gap, so I am able fully go on with my works.

I had the pleasure of collaborating with Cockcroft Institute that gives me lectures in physics accelerator by excellent lecturers from Lancaster University, University of Manchester, University of Liverpool, and STFC ASTeC Staff.

Lastly, I’d like to mention my family who always support, being by my side, and giving me a grateful instruction since I was a child that made me be me until now.

# Contents

Declaration . . . . .	i
Abstract . . . . .	ii
Acknowledgement . . . . .	iii
<b>1 Introduction</b>	<b>1</b>
1.1 Terahertz Radiation . . . . .	1
1.2 Terahertz Generators . . . . .	2
1.3 Corrugated Waveguide Structures . . . . .	4
1.4 Summary of a chapter 1 . . . . .	8
<b>2 Background Theory</b>	<b>9</b>
2.1 Particle-Field Interaction of Uniform Waveguides . . . . .	9
2.2 Uniform Waveguide Interpreted as a Periodic Structure . . . . .	11
2.3 Phase Velocity and Group Velocity . . . . .	13
2.4 Solution of Mathieu Equation: Floquet's Theorem . . . . .	15
2.5 Dispersion Relation and CIP . . . . .	21
2.6 Particle-Field Interaction of Corrugated Wave-guides . . . . .	23
2.7 Summary of a chapter 2 . . . . .	26
<b>3 Rectangular Corrugated Waveguide</b>	<b>27</b>
3.1 Electric Field and Magnetic Field . . . . .	27
3.2 Numerical Solution of a Rectangular Corrugated Waveguide . . . . .	31
3.3 Summary of a chapter 3 . . . . .	35
<b>4 Theory of the Cylindrical Corrugated Waveguide</b>	<b>36</b>
4.1 Electric Field and Magnetic Field . . . . .	36
4.2 The Error Max ( $\varepsilon_{Max}$ ) Minimization . . . . .	37
4.3 Boundary Conditions . . . . .	37
4.4 Mathieu Equation of the Cylindrical Corrugated Waveguide . . . . .	38
4.5 The Ansatz Optimization . . . . .	40
4.6 Summary of a chapter 4 . . . . .	42
<b>5 CST Simulation of the Cylindrical Corrugated Waveguide</b>	<b>43</b>
5.1 Set Up the Conditions for Simulation . . . . .	43
5.2 Analytical and Numerical Results Comparison . . . . .	47
5.3 Phase and Group Velocities . . . . .	51
5.4 Variation of $\delta$ and $q$ . . . . .	54
5.5 Summary of a chapter 5 . . . . .	56
<b>6 Future Works</b>	<b>57</b>

*CONTENTS*

---

<b>7 Conclusion</b>	<b>59</b>
<b>A Create a Structure</b>	<b>60</b>

# List of Figures

1.1	The interaction regimes of electrons and an electric field of TWTs and the changes in amplitude of an electric field. . . . .	3
1.2	The examples of various corrugated structure profiles. . . . .	4
1.3	The cross-section height of symmetric corrugated waveguide profile. . . . .	4
1.4	The dispersion relation of rectangular corrugated waveguide. . . . .	5
1.5	3D model of the cylindrical corrugated waveguide by CST simulation. . . . .	7
2.1	An infinite uniform waveguide interpreted as a periodic structure. . . . .	11
2.2	The dispersion relation of periodic structure. . . . .	13
2.3	Comparison of Dispersion relation between a periodic structure and a uniform waveguide . . . . .	14
2.4	The dispersion relation with the fixed $\omega_c$ and varying $q$ . . . . .	19
2.5	The dispersion relation with the fixed $q$ and varying $\omega_c$ . . . . .	20
2.6	The Dispersion relation of the rectangular corrugated waveguide with the values of the CIP. . . . .	22
2.7	The relation between $q$ and $\hat{\omega}_c$ , and $q$ and $\beta_c$ . . . . .	23
2.8	A graph of the force felt by particles and traveling distance . . . . .	24
2.9	A graph of kinetic energy change of particles traveling along a rectangular waveguide . . . . .	25
3.1	The rectangular corrugated waveguide profile. . . . .	27
3.2	The rectangular corrugated profile with the variation in parameter $q$ and $L_0$ . . . . .	30
3.3	The rectangular corrugated waveguide profile $q = 0.1$ , $\omega_c = 1.254$ in CST . . . . .	31
3.4	A graph of normalized longitudinal electric field $TM_{11}$ mode and distance in z-direction . . . . .	32
3.5	The dispersion relation of the rectangular corrugated waveguide $q = 0.1$ , $\omega_c = 1.254$ . . . . .	33
3.6	Phase and group velocities of the rectangular corrugated waveguide $q = 0.1$ , $\omega_c = 1.254$ . . . . .	34
3.7	Dispersion relation and phase and group velocities of the rectangular corrugated waveguide $q = 0.1$ , $\omega_c = 1.06$ . . . . .	34
4.1	The cylindrical corrugated profile when varying parameter $q$ and $R_0$ . . . . .	40
5.1	For a Background Properties setup, chose Material type to be PEC. . . . .	44
5.2	For a Boundary Conditions setup, choose “electric ( $E_t = 0$ )” in all directions. . . . .	44

5.3	For a Boundary Conditions setup, choose “electric ( $Et = 0$ )” in all directions. . . . .	45
5.4	For a Boundary Conditions setup, choose “electric ( $Et = 0$ )” in all directions. . . . .	45
5.5	For Eigenmode Solver Parameters. . . . .	45
5.6	The example of the $TM_{01}$ mode electric field simulated by CST. . . .	46
5.7	The graph of a normalized longitudinal electric field and $z$ , plotting from data of a simulation fig.5.6. . . . .	46
5.8	A graph of the normalized longitudinal electric field $TM_{01}$ mode of the cylindrical corrugated waveguide and distance in $z$ -direction . . .	48
5.9	The dispersion relation of the cylindrical corrugated waveguide $q = 0.1, \omega_c \approx 1.255$ . . . . .	49
5.10	A graph of the normalized longitudinal electric field $TM_{01}$ mode of the cylindrical corrugated waveguide and distance in $z$ -direction in $x - y$ cross-section. . . . .	50
5.11	Phase and group velocities of the cylindrical corrugated waveguide $q = 0.1, \omega_c \approx 1.225$ . . . . .	51
5.12	Phase and group velocities of the cylindrical corrugated waveguide $q = 0.1, \omega_c \approx 1.086$ . . . . .	52
5.13	The dispersion relation of the cylindrical corrugated waveguide $q = 0.1, \omega_c \approx 1.086$ . . . . .	52
5.14	A graph of the normalized longitudinal electric field $TM_{01}$ mode of the cylindrical corrugated waveguide and distance in $z$ -direction with differences in $\delta$ . . . . .	54
5.15	A graph of the normalized longitudinal electric field $TM_{01}$ mode of the cylindrical corrugated waveguide and distance in $z$ -direction with differences in $q$ . . . . .	55
A.1	Create the cylindrical corrugated waveguide fig.A.1 . . . . .	60
A.2	Create the cylindrical corrugated waveguide fig.A.2 . . . . .	61
A.3	Create the cylindrical corrugated waveguide fig.A.3 . . . . .	61
A.4	Create the cylindrical corrugated waveguide fig.A.4 . . . . .	61
A.5	Create the cylindrical corrugated waveguide fig.A.5 . . . . .	62
A.6	Create the cylindrical corrugated waveguide fig.A.6 . . . . .	62
A.7	Create the cylindrical corrugated waveguide fig.A.7 . . . . .	62
A.8	Create the cylindrical corrugated waveguide fig.A.8 . . . . .	63

# List of Tables

1.1	Electromagnetic spectrum indicating terahertz in gray. . . . .	1
2.1	The table selected sample of $q$ , and $\hat{\omega}_c$ and their CIP. . . . .	22
5.1	Collection of data from the analytical and numerical result of the cylindrical corrugated waveguide $q = 0.1$ , $\omega_c \approx 1.254$ . . . . .	49

# Chapter 1

## Introduction

### 1.1 Terahertz Radiation

Electromagnetic radiation is the emission or the transferring of energy in the form of photons or electromagnetic waves. Electromagnetic radiation's wavelength can span practically from 0 to nearly infinity, and can be used in various purpose. The table 1.1 shows electromagnetic spectrum categorized by frequency and wavelength ranges.

Spectral name	Wavelength	Frequency (Hz)
Radio waves	$\geq 1$ m	$3 - 3 \times 10^8$
Microwaves	1 m - 1 mm	$3 \times 10^8 - 3 \times 10^{11}$
Terahertz	3 mm - 30 $\mu$ m	$3 \times 10^{11} - 10^{13}$
Infrared	1 mm - 750 nm	$3 \times 10^{11} - 4 \times 10^{14}$
Visible light	750 nm - 400 nm	$4 \times 10^{14} - 8 \times 10^{14}$
Ultraviolet	400 nm - 1 nm	$10^{15} - 10^{17}$
X-rays	1 nm - 1 pm	$10^{17} - 10^{20}$
Gamma Rays	1 pm - 0.0001 pm	$10^{20} - 10^{24}$

Table 1.1: Electromagnetic spectrum indicating terahertz in gray.

These spectral bands are produced by a wide variety of generators. For instance; microwave can be produced by klystron and magnetron. However, there is a range of frequencies that these technologies cannot approach. The electrical technologies for generating microwave radiation, e.g. traveling tubes that can generate radiation need to be scaled down to sub-millimeters so they are able to produce radiation in the range of terahertz. This requires the precise micro-fabricated technologies to build these devices.

Because of the limitation of technologies for generating the radiation, there is still range of frequencies that these technologies cannot generate. This range is called "Terahertz gap[1]" which refers to frequencies 0.3 – 10 THz (wavelengths are in range 3 mm to 30  $\mu$ m).

Terahertz radiation or sub-millimeter radiation wavelengths lie in the range between microwave and infrared. With the non-ionizing property, terahertz radiation

can penetrate non-conductive materials. Nevertheless, terahertz radiation can be absorbed by water, this makes terahertz unable to penetrate water, plus it can only travel with a short distance through fog or cloud which consists of water vapor[2]. Because of this reason, terahertz sources are rarely found in nature.

These properties of terahertz are exploited to be used in a variety of applications. For example, because of its non-ionizing property, terahertz radiation is safe for imaging and screening applications, in contrast to X-ray which risks causing cancer in the human body. Terahertz Pulsed Imaging (TPI) is a non-invasive and non-destructive medical imaging technique which can be used to expose breast tumors harmlessly in humans with the low power approximately 100 nW, in frequency range 0.1 – 3.0 THz[3]. Another example in this area is the imaging of skin cancer, using terahertz in frequency range of 0.1 – 2.7 THz, average power 1 mW[4]. Furthermore, the non-conduction materials penetration property makes terahertz useful for security applications. Terahertz in range 0.5 – 10 THz is used to detect metallic weapons, explosives and illicit drugs by analyzing its spectrum characteristic[5]. In addition, communication technology tends to shift from fifth-generation (5G) to sixth-generation (6G) communications[6] which uses the frequencies range in terahertz. Hence terahertz is high frequency wave, this gives it an advantage in a high transmission rate. However, because of the quick attenuation in the air containing with molecules of water, terahertz are used for short-distance wireless communications.

The development of terahertz generators can open the opportunities for improving current innovation or new technologies to be more effective. The reinvigoration of the interested in terahertz radiation and generators started in 1994 with the publication of quantum cascade laser (QCL)[7] which can generate wavelengths from the mid-infrared to the sub-millimeter wave (terahertz frequency). This and other researches in late twentieth century opened the door to the study in the terahertz radiation research field.

## 1.2 Terahertz Generators

Since 1990s, numerous methods have been developed to produce terahertz. They can be categorized into 3 main methods; femtosecond laser excitation including, photoconductive antennas (PCAs), nonlinear crystals or optical rectification, and laser- induce gas plasma. The second method is solid state devices such as QCLs. Another method is electronics and accelerators, for example; vacuum electronics devices (VEDs).

The first laser-based terahertz pulse is the photoconductive antennas[8] in 1984 and then developed to the large aperture photoconductive antennas (LAPCAs)[9] in 1993 with the aperture size 3.5 cm, which are able to generally generate low terahertz frequencies in range between 0.1 and 1 THz. The optical rectification generate frequencies band from 0.1 THz to 6 THz depending on the types of nonlinear crystal. Both LAPCAs and optical rectification has the advantage in producing high stability terahertz radiation, however there is the limitation which could occur from laser damage[10].

In addition to these various techniques, other well-known and cost effective methods of terahertz generation are vacuum electronics devices (VEDs)[11]. VEDs are devices consisting of the vacuum tube connected to the electron source which emit

the electrons to be interacted by an electromagnetic wave through the vacuum tube.

VEDs can be divided into 2 groups, transverse modulation and longitudinal modulation of the current[12]. The transverse modulation current devices exploit a magnetic field to modulate an electron's velocity perpendicularly from its primary axis. One remarkable technology for this type of VEDs is the Free Electron Laser (FEL)[13]. The machine works by guiding a bunch of electrons through an undulator to generate radiation. For the research of producing radiation, FEL is one of the most reliable method. Since they can produce high intensity, coherent light, not only terahertz radiation is generated but also a broad range of wavelengths from long (microwave) all the way to short wavelengths (X-ray). Considering the idea of constructing the FEL in Thailand, there certainly would be advantages from using such a machine, e.g., drug manufacturing, heavy manufacturing and also academic research. The construction of FEL in Thailand powered by synchrotron will boost the economy and research areas. Nevertheless, FEL requires large amounts of funding and numerous researchers to work on this machine.

The longitudinal current modulation devices utilize an electric field component of an electromagnetic wave to induce a longitudinal modulation of an electron's velocity in the same direction with the primary axis. For example, the backward-wave oscillators (BWOs)[14] use a backward traveling electric field against an electron beam, this causes the deceleration of electrons, and radiation is generated from this deceleration. Another example is the traveling-wave tubes (TWTs)[15]. In contrast to BWOs, TWTs use a forward traveling electric field to interact with an electron beam. TWTs are used as an amplifier for radio frequency (RF) signals from microwave up to terahertz frequencies. When electrons enter an electric field, they experience different regions of a field (accelerating regions and decelerating regions). The electrons which fall into decelerating region lose their kinetic energy, and this energy is transferred to an electric field which leads to an increasing of a wave's amplitude. At some point where electrons lose their kinetic energy and cannot keep their velocity synchronism with a wave's velocity, bunches of electrons start to disperse and there is no longer the growth in a wave's amplitude as shown in fig.1.1.

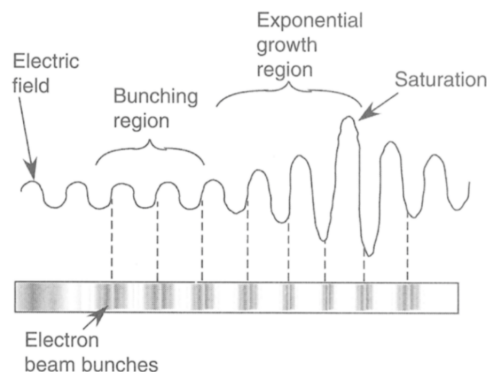


Figure 1.1: The interaction regimes of electrons and an electric field of TWTs and the changes in amplitude of an electric field.

For this research, we study a cylindrical corrugated waveguide used in TWTs which continues work from the research in a rectangular corrugated waveguide[16]. The corrugated profile makes this structure different from other conventional waveguides which have a uniform profile. These corrugations can slow down the phase

velocity of electromagnetic waves which propagate through the structure. The structures that have this characteristic are known as “slow-wave structures (SWSs)”. Because the phase velocity of an electromagnetic wave is slower than the velocity of light, this allows electrons to interact with an electric field. If electrons are decelerated, radiation is generated (SWSs are also used in BWOs for generating radiation). If electrons travel along an electric field, electrons that experience decelerating regions will lose their kinetic energies and amplify an amplitude of an electric field (TWTs are used to amplify RF signals).

### 1.3 Corrugated Waveguide Structures

The research community shows the interest in corrugated waveguide profiles. For example; sine waveguide (SWG)[17], flat-roofed sine waveguide (FR-SWG)[18], and piecewise sine waveguide (PW-SWG)[19]. However, only the PW-SWG is able to generate radiation in the terahertz range.

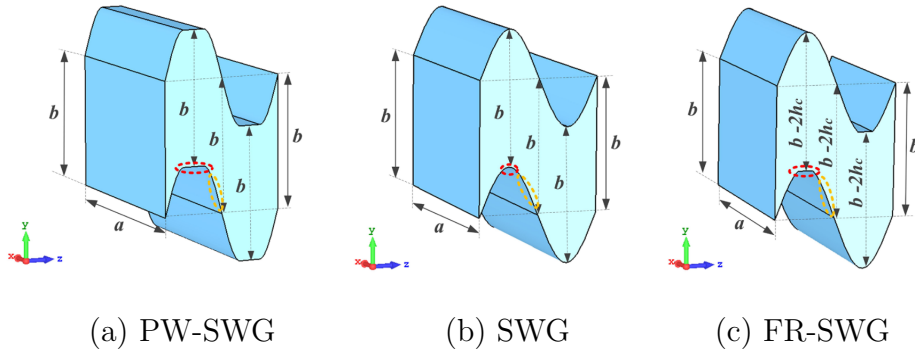


Figure 1.2: Adapted figure from [19]. The image exhibit the examples of various corrugated structure profiles. With slight difference in shape (a) PW-SWG is improved from SWG and FR-SWG with the property of maximizing particle-wave interaction because of the lower distribution caused by sine walls. (b) SWG has the advantages in wide bandwidth, electron beam tunnel, and easy to manufacture. (c) FR-SWG can work in the W-band (77 – 110 GHz regarding Institute of Electrical and Electronics Engineers (IEEE)).

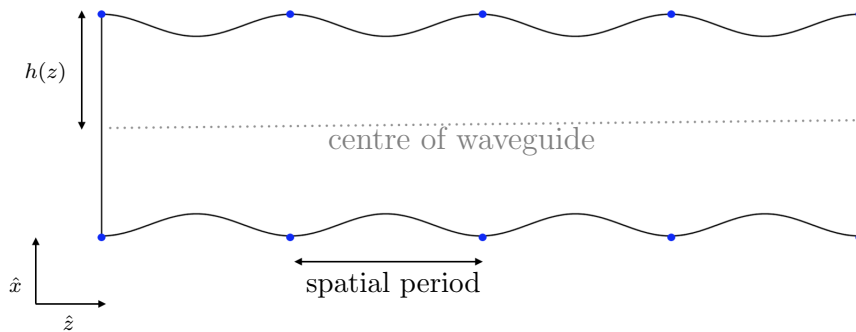


Figure 1.3: The cross-section height of symmetric corrugated waveguide profile in this research.

The corrugated wall profiles of the two corrugated waveguides which will be studied in this thesis; the rectangular corrugated waveguide in chapter 3, and the cylindrical corrugated waveguide in chapter 4, are different from the previous research especially the sine waveguide. Instead of the upper and lower walls simultaneously oscillating up and down along longitudinal direction ( $z$  axis), this corrugated waveguide has symmetrical corrugation (the top and bottom corrugation are reflections of each other) in a cross-section height as shown in fig.1.3. The height of the corrugated waveguide  $h(z)$  is a periodic function to  $z$ . Particles would travel at the center of the waveguide ( $x = 0, y = 0$ ) where there is only an electric field. There are 2 remarkable advantages for this specific corrugated structure. Firstly, the corrugation of the structure is shallow and this makes the huge difference from other slow-wave structures e.g., radio frequency (RF) cavity. For our corrugated waveguide, the explicit approximate solutions of the electromagnetic waves can be solved by Mathieu's functions. With these solutions, the designing of the structure corresponding to desirable properties (e.g., particle velocity, cut-off frequency, and electromagnetic field modes) can be more easily achieved compared to other VEDs. Secondly, we have defined the point on the dispersion relation of the symmetrical corrugated waveguide where particles not only interact with an electric field but also interact in the wide range of frequencies. This point is called "coincident inflection point (CIP)", see fig.1.4.

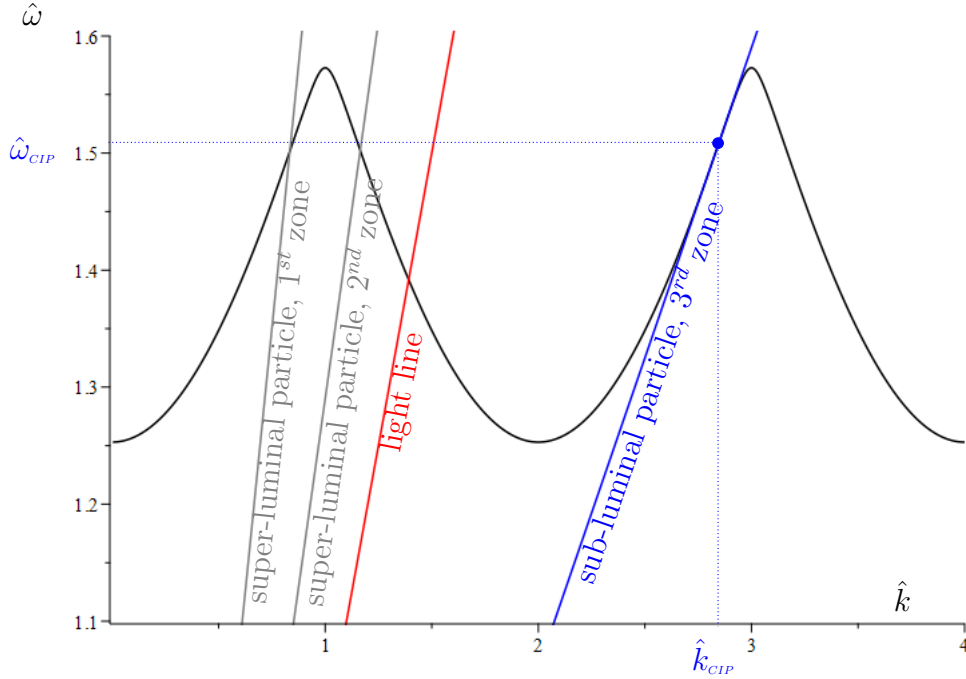


Figure 1.4: Reproduced figure from [16]. The dispersion relation of the rectangular corrugated waveguide. A red line is the velocity of light. Gray lines present particles which have velocities greater, than light. A blue line represent particles traveling with a velocity less than the light velocity. A blue dotted line is the angular frequency of CIP.

The dispersion relation of the symmetrical corrugated waveguide in fig.1.4 can be classified into 3 regions; the 1<sup>st</sup> are always the "super-luminal" where the particle velocity is greater than the light velocity, the 2<sup>nd</sup> is often the "super-luminal"

depending on the parameters. The 3<sup>rd</sup> is “sub-luminal” where the particle velocity is less than the light velocity.

For determining the CIP of the dispersion relation, there are 3 conditions that need to be considered.

1. A particle can be interacted with an electric field which has a phase velocity less than the light velocity. A phase velocity of an electromagnetic field need to be equal to a particle’s velocity and both must be less than the light velocity.

$$\frac{\hat{\omega}_{CIP}}{\hat{k}_{CIP}} = \beta_e \quad (1.1)$$

where  $\hat{\omega}_{CIP}$  and  $\hat{k}_{CIP}$  are a normalized angular frequency and a normalized wavenumber of the CIP, respectively.

2. To avoid a dispersion of an electromagnetic field, a group velocity and a phase velocity need to be equal.

$$\frac{\hat{\omega}_{CIP}}{\hat{k}_{CIP}} = \frac{d\hat{\omega}_{CIP}}{d\hat{k}_{CIP}} \quad (1.2)$$

3. Due to a frequency of electromagnetic field is not monochromatic, it is beneficial to satisfy a zero group velocity dispersion (GVD) which is an inflection point on the dispersion to allow the particle-field interaction in a broad range of frequencies.

$$\frac{d^2\hat{\omega}_{CIP}}{d\hat{k}_{CIP}^2} = 0 \quad (1.3)$$

The normalized angular frequency  $\hat{\omega}$  and the normalized wavenumber  $\hat{k}$  that can satisfy these 3 conditions are “CIP”. At this point, a particle would interact with the wide range frequencies of an electric field with the synchronous phase velocity. With these advantages, they help to enhance efficiency of amplifying RF signals by our corrugated waveguide at specific frequency.

In this thesis, we will investigate the symmetrical corrugated structure which has a cylindrical profile fig.1.5. The cylindrical corrugated waveguide is a developed structure from the rectangular corrugated waveguide[16]. The cylindrical corrugated waveguide surpasses the rectangular in terms of reducing cost in manufacturing because of relatively easy fabrication process. The size of the waveguide is an inversely proportion to a frequency of an electromagnetic wave. Therefore, high frequencies require a small waveguide. The corrugated waveguide which has rectangular cross-section profile (e.g., [17], [18], [19], and [16]) can be made by micro-fabrication technologies[20], e.g., lithographic techniques which can make a waveguide circuit in a sub-millimeter scale, or computer numerical control (CNC)[21] which achieves a building of waveguide circuit generating frequencies 300 GHz and above. On the other hand, the cylindrical corrugated waveguide can be fabricated in a similar way to fiber optic by the extrusion technique[22]. The process has 2 steps. First step is molding glass into the corrugated shape, the heated glass is extruded to make the undulated shape. The radius and a period of a corrugation can be designed by varying the speed of an extrusion, relatively low speed can make the radius bigger and a corrugation’s period shorter than a high speed extrusion. The next step is

covering the cylindrical corrugated glass with silver which is the conducting material, and using the chemical solvent to dissolve the glass. The resulting product from this process will be silver in the shape of cylindrical corrugation which is a conducting waveguide. This process hopefully requires a lower cost than lithographic techniques. If the manufacturing of the cylindrical corrugated waveguide is low and uncomplicated, this could lead to commercially available terahertz products that are accessible to all.

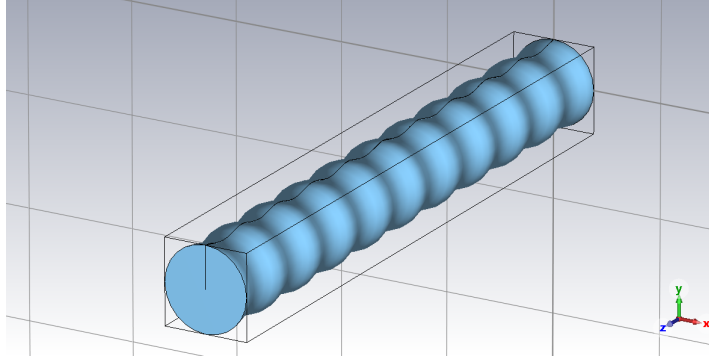


Figure 1.5: 3D model of the cylindrical corrugated waveguide by CST simulation.

For the next chapter, chapter two cover background theory. We discuss a phase and a group velocity of waveguides in general, followed by a particle-field interaction for a uniform waveguide. We interpret the uniform waveguide as a periodic structure and examine its dispersion relation. Then, we discuss the solution of Mathieu equation, the Floquet's Theorem which is the important part for finding the analytical results of electromagnetic fields for our structures and designing our waveguides' profile. Finally we discuss on the dispersion relation of our symmetric corrugated waveguides both the rectangular and the cylindrical corrugated waveguide and their CIP.

In chapter three, building from the work by [16], we investigate the structure of the rectangular corrugated waveguide. This includes the analytical solution and geometry parameters that correspond to Floquet theorem. By comparing the analytical solution and the numerical solution from the CST simulation, we can tell how good our approximate results are.

In chapter four, we develop the analytical solution from chapter three. Instead of the rectangular corrugated waveguide, we find the analytical solution of the cylindrical corrugated waveguide in detail, including optimizing the approximate results by reducing the errors.

In chapter five, we show the numerical results from the CST of the cylindrical corrugated waveguide and compare them with the analytical results from chapter four.

This is followed by the discussion and future works and finally the conclusion of this project.

## 1.4 Summary of a chapter 1

In section 1.1, we discuss on the terahertz radiation which has frequencies lie within a range  $0.3 - 10$  THz and their properties, e.g., the non-ionizing property, high frequency wave. With these properties, terahertz is exploited in wide areas, such as medical imaging, security detector (detecting weapon, explosives, drugs), and communication (6G).

There are 3 methods for producing terahertz in section 1.2. The first method is femtosecond laser excitation, the second method is solid state devices, and the last method is electronics and accelerators (our structure, the cylindrical corrugated waveguide is included in this group). We study the cylindrical corrugated waveguide which is the traveling-wave tube (TWT) which is used for amplifying signals from microwave to terahertz frequencies. To amplify signals, there must be an interaction between particles and an electric field. The structures that permits particles-fields interaction are a slow-wave structures (SWSs).

The rectangular and cylindrical corrugated waveguide (Chapter 3 and Chapter 4) are slow-wave structures (SWSs) which have the symmetric corrugated profile. This unique profile provides us the advantages. Firstly, by designing the corrugated wall to be smooth (shallow corrugation), we can find the explicit approximate solutions of the electromagnetic waves. For another advantage, we define the “coincident inflection point (CIP)” where the particles travel with the velocity synchronizing to a phase velocity of an electric field, plus these particles would interact with wide range frequencies of an electric field.

In addition, the method of producing the cylindrical corrugated waveguide is the extrusion technique. By varying the speed of heated glass extrusion, the corrugation profile is produced. We expect this process has less cost and is easier to produce than the rectangular corrugated waveguide which uses computer numerical control (CNC).

# Chapter 2

## Background Theory

### 2.1 Particle-Field Interaction of Uniform Waveguides

To amplify electromagnetic waves in TWTs, there must be the exchange of energy between kinetic energy of a particle and an electromagnetic wave. Therefore, when a particle travels through a waveguide, they must lose energy to an electric field inside a waveguide. The corrugated structure is a slow-wave structures (SWSs) that can permit a phase velocity of a propagating electric field (considering  $\text{TM}_{11}$  mode for the rectangular waveguide, and  $\text{TM}_{01}$  mode for the cylindrical waveguide, at the center where there is only an electric field) along waveguides to be lower than the velocity of light. This property allows particles to interact and exchange energy with an electric field by being accelerated or decelerated by an electric force. On the other hand, uniform waveguides have phase velocities more than the velocity of light, particles cannot travel with velocities more than the velocity of light. Therefore, there is no energy exchanges in uniform waveguides.

In this chapter, we will show that there is no energy transferring between traveling particles and an electric field in uniform waveguides. For corrugated waveguides, we will discuss this energy gain in section 2.6 which is symmetric corrugated structures.

Let us consider an inverse Fourier transform of an electric field in the frequency domain.

$$\mathbf{E}(t, z) = \frac{1}{2\pi} \text{Re} \left[ \int \tilde{\mathbf{E}}(\omega, z) e^{-i\omega t} d\omega \right] \quad (2.1)$$

Where  $\tilde{\mathbf{E}}(t, z)$  is an electric field in the time domain at a time  $t$  and a position  $z$ ,  $\tilde{\mathbf{E}}(\omega, z)$  is an electric field in the frequency domain at frequency  $\omega = 2\pi f$  and a position  $z$ .

Let us first consider the ordinary cylindrical waveguides with uniform profile, the electric field for  $\text{TM}_{01}$  mode in  $z$ -direction along the center of waveguides is

$$\mathbf{E}(\omega, z) = E_0 e^{ik_z z} \quad (2.2)$$

$E_0$  is an amplitude and  $k_z$  is a wavenumber of electric field for  $\text{TM}_{01}$  mode in  $z$ -

direction. Then the electric field in time domain of eq.2.2 is

$$\mathbf{E}(t, z) = \frac{1}{2\pi} \text{Re} \left[ \int E_0 e^{ik_z z} e^{-i\omega t} \rho(\omega) d\omega \right] \quad (2.3)$$

where  $\rho(\omega)$  is the spectral density of an electric field. For a monochromatic field that an electric field carries only one value of frequency, then  $\rho(\omega) = \delta(\omega - \omega_s)$  at the phase-matched frequency  $\omega_s$ .

If a particle with velocity  $v_p = \frac{\omega}{k_z} = c\beta_e$  enters a waveguide at a time  $t_0$  and at a position  $z_0$ , after a time passes to  $t_p = t_0 + \frac{z_p}{c\beta_e}$ , a particle will be at a position  $z_p$ .

With these conditions, eq.2.3 becomes

$$\begin{aligned} \mathbf{E}(t_p, z_p) &= \frac{1}{2\pi} \text{Re} \left[ \int E_0 e^{ik_z z_p} e^{-i\omega t_p} \rho(\omega) d\omega \right] \\ &= \frac{1}{2\pi} E_0 \text{Re} \left[ \int e^{ik_z z_p} e^{-i\omega t_p} \delta(\omega - \omega_s) d\omega \right] \\ &= \frac{1}{2\pi} E_0 \text{Re} \left[ e^{ik_z z_p} e^{-i\omega_s t_p} \right] \\ &= \frac{1}{2\pi} E_0 \text{Re} \left[ e^{i(k_z z_p - \omega_s t_p)} \right] \\ &= \frac{1}{2\pi} E_0 \text{Re} \left[ \cos(k_z z_p - \omega_s t_p) - i \sin(k_z z_p - \omega_s t_p) \right] \\ &= \frac{1}{2\pi} E_0 \cos(k_z z_p - \omega_s t_p) \end{aligned} \quad (2.4)$$

The total changes in energy ( $\Delta e_p$ ) of a particle traveling over a period of the structure  $L_z = 2\pi$ , is the integrated of an electric force

$$\begin{aligned} \Delta e_p &= q \int_0^{L_z} \mathbf{E}(t_p, z_p) dz_p \\ &= \pi^{-1} q E_0 \int_0^{2\pi} \cos(k_z z_p - \omega_s t_p) dz_p \\ &= 0 \end{aligned} \quad (2.5)$$

The total changes in energy equals to 0 in uniform waveguides. This means particles cannot exchange an energy with an electric field in uniform waveguides. Therefore, we cannot amplify terahertz radiation by uniform waveguides.

## 2.2 Uniform Waveguide Interpreted as a Periodic Structure

In this section, we will show that a periodic structure—a slow-wave structure, can slow down a phase velocity of electromagnetic waves. A phase velocity of electromagnetic waves is lower than the velocity of light because electromagnetic waves reflect with the periodic element. As a result of this reflection, the dispersion relation curve repeats itself every certain period of a wavenumber.

Considering a uniform waveguide in the frequency domain, at the center ( $x = 0$ ,  $y = 0$ ) there is only a longitudinal component of an electric field  $E_z(z)$

$$E_z(z) = e^{-ik_z z} \quad (2.6)$$

$k_z$  is a wavenumber of an electric field in z-direction, then the dispersion relation of a uniform waveguide is

$$\omega = c(k_z^2 + a^2)^{1/2} \quad (2.7)$$

where  $\omega$  is an angular frequency, and  $a$  is a cut-off frequency.

We interpret an infinite uniform waveguide as a periodic structure, between a unit cell with a period  $L_z$  as shown in fig.2.1

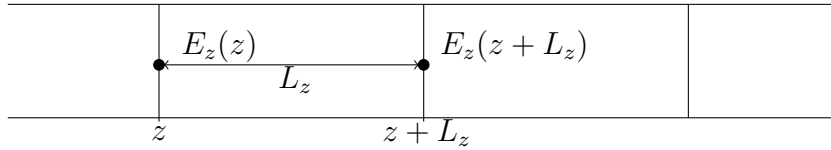


Figure 2.1: An infinite uniform waveguide interpreted as a periodic structure.

Regarding Floquet theorem, the change in a longitudinal electric field from any position  $z_0$  in a unit cell to the same position in a next unit cell can be expressed by an exponential term

$$E_z(z + L_z) = e^{-ik_z L_z} E_z(z) \quad (2.8)$$

an electric field that can satisfy eq.2.8 is

$$E_z(z) = e^{-ik_z z} P(z) \quad (2.9)$$

where  $P(z)$  is a periodic function with a period  $L_z$ ,  $P(z + L_z) = P(z)$  and can be written as a complex Fourier series

$$P(z) = \sum_{n=-\infty}^{+\infty} C_n e^{i\frac{2n\pi}{L_z} z} \quad (2.10)$$

$n$  is integers from  $-\infty$  to  $+\infty$ , and  $C_n$  is a complex Fourier coefficient.

$$C_n = \frac{1}{2L_z} \int_{-L_z}^{L_z} P(z) e^{-i\frac{2n\pi}{L_z} z} dz \quad ; n \in \mathbb{Z} \quad (2.11)$$

Substitute  $P(z)$  eq.2.10 into eq.2.9

$$\begin{aligned}
 E_z(z) &= e^{-ik_z z} P(z) \\
 &= e^{-ik_z z} \sum_{n=-\infty}^{+\infty} C_n e^{i\frac{2n\pi}{L_z} z} \\
 &= \sum_{n=-\infty}^{+\infty} C_n e^{-ik_z z + i\frac{2n\pi}{L_z} z} \\
 &= \sum_{n=-\infty}^{+\infty} C_n e^{-i(k_z - \frac{2n\pi}{L_z})z} \\
 &= \sum_{n=-\infty}^{+\infty} C_n e^{-ik_{zn} z}
 \end{aligned} \tag{2.12}$$

we defined a new variable  $k_{zn}$

$$k_{zn} = k_z - \frac{2n\pi}{L_z} \quad ; n \in \mathbb{Z} \tag{2.13}$$

From eq.2.12 for a uniform waveguide interpreted as a periodic waveguide, there are an infinite number of traveling waves, called space harmonics[23] (denoted by index  $n$ ) and  $k_{zn}$  in eq.2.13 is a wavenumber of each space harmonic  $n$ . When  $n = 0$ , the traveling wave is the principle wave which is the dominant field. Waves travel in  $+z$  direction when  $n > 0$  and travel in  $-z$  direction when  $n < 0$ .

Substituting  $k_{zn}$ , eq.2.13 into eq.2.7, to derive the dispersion relation of a periodic structure

$$\begin{aligned}
 \omega &= c(k_{zn}^2 + a^2)^{1/2} \\
 &= c\left(\left(k_z - \frac{2n\pi}{L_z}\right)^2 + a^2\right)^{1/2} \quad ; n \in \mathbb{Z}
 \end{aligned} \tag{2.14}$$

The dispersion relation of a periodic structure in fig.2.2 shows the principle wave  $n = 0$  and harmonic waves  $n = -2, -1, 1, 2$ . Because a period of this structure is  $L_z = \pi$ , a wavenumber of each harmonic wave shifts every  $k + 2$ . For large values of  $k$ , electric fields can propagate with low frequencies. This allows a phase velocity of electric field less than the light velocity. However, because we indicated this periodic condition in a uniform waveguide, there are no energy gains from this structure.

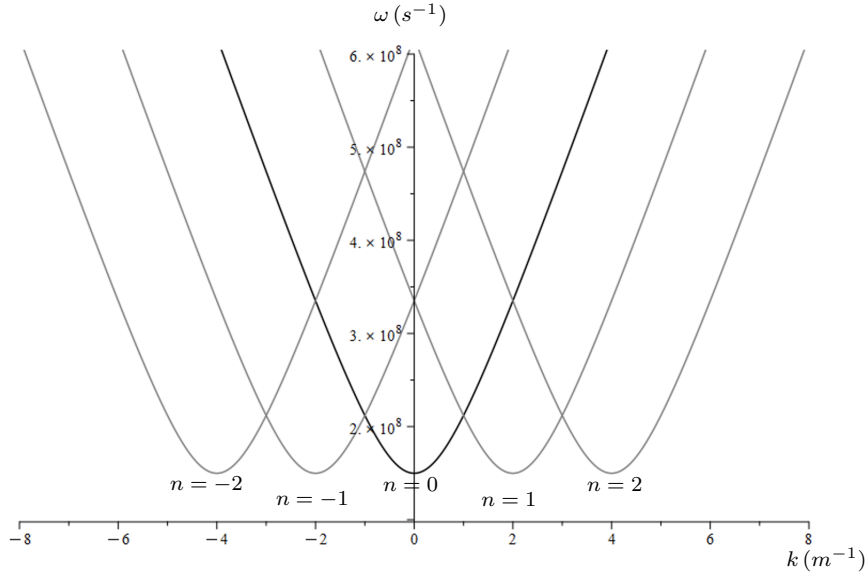


Figure 2.2: The dispersion relation of periodic structure shows dispersion graph of principle wave  $n = 0$  and harmonic waves  $n = -2, -1, 1, 2$ . In the corrugated waveguide, the crossing in this figure open up for the band gaps as in fig.2.4 and fig.2.5.

## 2.3 Phase Velocity and Group Velocity

We look at particles which enter at a center of a waveguide,  $x = 0$  and  $y = 0$ , where there is only an electric field in  $z$ -direction  $\mathbf{E}(\omega, z) = E_0 e^{ik_z z}$ . After particles entering a waveguide, an electric field interacts with particles, an electric force accelerates particles to travel along the waveguide. The important condition of accelerating particles with an electric field that needs to be considered is a velocity of a particle, a phase and a group velocity of an electromagnetic wave in a waveguide.

Waves in nature consist of waves with different frequencies and wave numbers, there are no truly monochromatic waves which means waves with only one frequency [24]. These broadband waves are consisted of wave packets. A wave group propagates in space with a group velocity,  $v_g = \frac{d\omega}{dk}$  and a phase velocity of component waves is  $v_p = \frac{\omega}{k}$ .

For waves propagating in waveguides, the relation between a phase and a group velocity of a wave group can be represented with a plot, called “dispersion relation”, as shown in fig.2.3b. Waves are allowed to propagate in waveguides with frequency above a cut-off frequency. Therefore, there are no waves propagating under the dispersion relation curve. A phase velocity of waveguides is a slope of a line from an origin to a point on a dispersion curve  $v_p = \frac{\omega}{k}$ , and a group velocity is derivative at a point on a dispersion curve  $v_g = \frac{d\omega}{dk}$ . For uniform waveguides in general, a phase velocity is faster than the velocity of light.

To gain the most efficient particle acceleration, a phase and a group velocity need to be equal. This makes wave groups remain the same shape through a waveguide, and particles are always interact with an electric field at its amplitude throughout the acceleration.

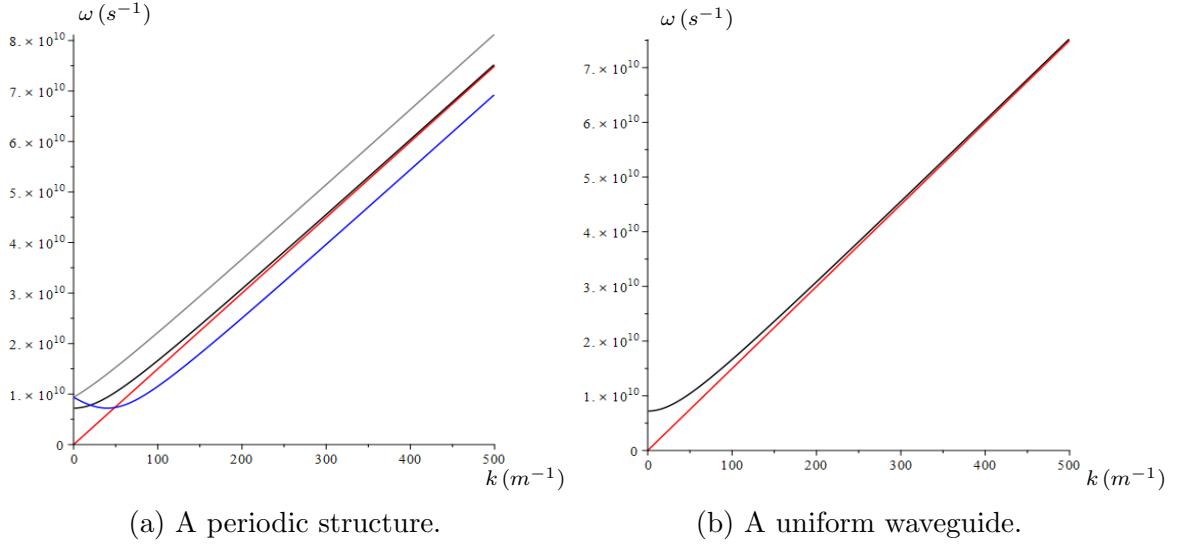


Figure 2.3: Dispersion relation of a uniform waveguide indicated as a periodic structure (a) the black line is the principle wave  $n = 0$ , the gray and the blue line are harmonic waves  $n = -20$  and  $n = 20$  respectively. (b) Dispersion relation of a uniform waveguide. The red line in both figures is the light line.

In addition, particles can be accelerated when a phase velocity of electromagnetic wave is lower than the velocity of light. For fig.2.3, we shows that for a periodic structure, there are harmonic waves (eq.2.14 where  $n > 0$ ) that can propagate with a velocity lower than a velocity of light (the blue line of a harmonic wave  $n = 20$  has a phase velocity lower than a velocity of light).

In this study, we introduce the coincident inflection point (CIP) where a phase and a group velocity coincide, and at the point of inflection of the dispersion relation to allow particles to interact with a range of frequencies. We will utilize this CIP to determine the structure of the waveguide.

## 2.4 Solution of Mathieu Equation: Floquet's Theorem

For the symmetric corrugated structures both the rectangular and the cylindrical shape, the electromagnetic fields at the wall are perturbed because of the corrugated wall. So we begin solving Maxwell's equations with a magnetic field function from a uniform waveguide but with the addition of  $\phi(\eta z)$  for adjusting the field due to the perturbation.

For the rectangular corrugated waveguide TM mode

$$\begin{aligned} \tilde{\mathbf{B}}_{rec} = B_0 c^{-2} (-i\omega) \phi(\eta z) & \left( \kappa_y \cos(\kappa_x x) \sin(\kappa_y y) \mathbf{e}_x \right. \\ & \left. - \kappa_x \sin(\kappa_x x) \cos(\kappa_y y) \mathbf{e}_y \right) \end{aligned} \quad (2.15)$$

and the cylindrical corrugated waveguide TM mode

$$\tilde{\mathbf{B}}_{cyl} = B_0 c^{-2} (-i\omega) \phi(\eta z) J_1(r g(\eta z)) \mathbf{e}_\theta \quad (2.16)$$

So both magnetic fields and electric fields are approximate solutions of Maxwell's equations. After minimizing the error for a good approximation, we get  $\phi(\eta z)$  in the form of Ordinary Differential Equation (ODE)

$$\phi''(\zeta) + (a - 2q \cos(2\zeta)) \phi(\zeta) = 0 \quad (2.17)$$

which is the Mathieu's equation where  $\zeta = \eta z = (\pi/L_z)z$ ,  $\eta = \pi/L_z$ ,  $L_z$  is a period of a corrugated waveguide,  $a$  and  $q$  are real-value parameters.

The solution of Mathieu's equation eq.2.17 can be solved by Floquet Theorem which has the definition of  $\phi(\zeta)$  as

$$\phi_{a,q}(\zeta) = e^{i\hat{k}\zeta} \Psi_{a,q,\hat{k}}(\zeta) \quad (2.18)$$

$\phi(\zeta)$  is composed of a characteristic number  $e^{i\hat{k}\zeta}$  and  $\Psi_{a,q,\hat{k}}(\zeta)$  is a periodic function  $\Psi_{a,q,\hat{k}}(\zeta + \pi) = \Psi_{a,q,\hat{k}}(\zeta)$ .

We define the parameter  $a = \hat{\omega}^2 - \hat{\omega}_c^2$  where  $\hat{\omega} = (L_z \omega)/(\pi c)$  is a normalized angular frequency, and  $\hat{\omega}_c$  is a normalized cut-off angular frequency, for the rectangular corrugated waveguide  $\hat{\omega}_c = (L_z^2/L_0^2 + L_z^2/L_y^2)^{1/2}$  and for the cylindrical corrugated waveguide  $\hat{\omega}_c = (\chi_0^1 L_z)/(\pi R_0)$ .  $q$  can be determined as a depth of the corrugation, and  $\hat{k}$  is the Mathieu exponent and relates to the wavenumber  $k = \eta \hat{k} = \pi \hat{k}/L_z$ . These parameters  $a$ ,  $q$ , and  $\hat{k}$  are physical parameters that determine the geometry of the symmetric corrugated structures which will be discussed further in chapter 3 and chapter 4.

Periodic function  $\Psi_{a,q,\hat{k}}(\zeta)$  can be represented by the complex Fourier series.

$$\Psi_{a,q,\hat{k}}(\zeta) = \sum_{n=-\infty}^{\infty} c_n e^{2in\zeta} \quad (2.19)$$

where  $n$  is integers, and  $c_n$  is a complex Fourier coefficient.

$\phi(\zeta)$  in eq.2.18 can be written in the form of complex Fourier series

$$\begin{aligned}\phi_{a,q}(\zeta) &= e^{i\hat{k}\zeta} \sum_{n=-\infty}^{\infty} c_n e^{2in\zeta} \\ &= \sum_{n=-\infty}^{\infty} c_n e^{i(\hat{k}+2n)\zeta}\end{aligned}\tag{2.20}$$

substitutes eq.2.20 into Mathieu's equation eq.2.17

$$\begin{aligned}- \sum_{n=-\infty}^{\infty} c_n (k+2n)^2 e^{i(\hat{k}+2n)\zeta} + (a - qe^{2\zeta i} - qe^{-2\zeta i}) \sum_{n=-\infty}^{\infty} c_n e^{i(\hat{k}+2n)\zeta} &= 0 \\ \sum_{n=-\infty}^{\infty} [(a - (\hat{k} + 2n)^2) c_n e^{i(\hat{k}+2n)\zeta} - qc_n e^{i(\hat{k}+2n+2)\zeta} - qc_n e^{i(\hat{k}+2n-2)\zeta}] &= 0 \\ \sum_{n=-\infty}^{\infty} [(a - (\hat{k} + 2n)^2) c_n e^{i(\hat{k}+2n)\zeta} + (-qc_{n-1} - qc_{n+1}) e^{i(\hat{k}+2n)\zeta}] &= 0 \\ \sum_{n=-\infty}^{\infty} [-qc_{n-1} + (a - (\hat{k} + 2n)^2) c_n - qc_{n+1}] &= 0\end{aligned}\tag{2.21}$$

eq.2.21 can be written in an infinite matrix form

$$\begin{bmatrix} \dots & \dots & \dots & \dots & \dots & \dots & \dots \\ \dots & -q & 0 & 0 & 0 & 0 & \dots \\ \dots & a - (\hat{k} - 4)^2 & -q & 0 & 0 & 0 & \dots \\ \dots & -q & a - (\hat{k} - 2)^2 & -q & 0 & 0 & \dots \\ \dots & 0 & -q & a - \hat{k}^2 & -q & 0 & \dots \\ \dots & 0 & 0 & -q & a - (\hat{k} + 2)^2 & -q & \dots \\ \dots & 0 & 0 & 0 & -q & a - (\hat{k} + 4)^2 & \dots \\ \dots & 0 & 0 & 0 & 0 & -q & \dots \\ \dots & \dots & \dots & \dots & \dots & \dots & \dots \end{bmatrix} \begin{bmatrix} \dots \\ c_{-2} \\ c_{-1} \\ c_0 \\ c_1 \\ c_2 \\ \dots \end{bmatrix} = 0\tag{2.22}$$

from matrix equation in matrix.2.22, the coefficient of the series is

$$\begin{aligned}-qc_{n-1} + (a - (\hat{k} + 2n)^2)c_n - qc_{n+1} + 1 &= 0 \\ c_n &= \frac{q(c_{n+1} + c_{n-1})}{a - (\hat{k} + 2n)^2}\end{aligned}$$

When  $|n| \rightarrow \pm\infty$  then

$$\begin{aligned}\lim_{n \rightarrow \pm\infty} c_n &= \lim_{n \rightarrow \pm\infty} \frac{q(c_{n+1} + c_{n-1})}{a - (\hat{k} + 2n)^2} \\ \lim_{n \rightarrow \pm\infty} c_n &= 0\end{aligned}$$

This means  $c_n$  converges to 0 when  $|n| \rightarrow \pm\infty$ . So the infinite matrix in fig.2.22 can be truncated. to the finite matrix. Here we have chosen a  $5 \times 5$  matrix.

$$\begin{bmatrix} a - (\hat{k} - 4)^2 & -q & 0 & 0 & 0 \\ -q & a - (\hat{k} - 2)^2 & -q & 0 & 0 \\ 0 & -q & a - \hat{k}^2 & -q & 0 \\ 0 & 0 & -q & a - (\hat{k} + 2)^2 & -q \\ 0 & 0 & 0 & -q & a - (\hat{k} + 4)^2 \end{bmatrix} \begin{bmatrix} c_{-2} \\ c_{-1} \\ c_0 \\ c_1 \\ c_2 \end{bmatrix} = 0 \quad (2.23)$$

By comparing to a  $7 \times 7$  truncation, we can show that this is a good approximation for the values of  $q \approx 0.1$  which we are interested in.

To guarantee that Floquet's eq.2.18 has at least one non-trivial solution, the determinant of matrix in fig.2.23 must be equal to 0

$$\begin{vmatrix} a - (\hat{k} - 4)^2 & -q & 0 & 0 & 0 \\ -q & a - (\hat{k} - 2)^2 & -q & 0 & 0 \\ 0 & -q & a - \hat{k}^2 & -q & 0 \\ 0 & 0 & -q & a - (\hat{k} + 2)^2 & -q \\ 0 & 0 & 0 & -q & a - (\hat{k} + 4)^2 \end{vmatrix} = 0 \quad (2.24)$$

We have the relation between  $q$  and the geometry of structure,  $a = \hat{\omega}^2 - \hat{\omega}_c^2$ . By fixing the depth of corrugations  $q$  and a normalized cut-off angular frequency  $\hat{\omega}_c$ , then we can find the dispersion relation  $\hat{\omega} - \hat{k}$  of the structure from the determinant in eq.2.24.

In fig 2.4 we show how dispersion relation changes if  $q$  is varied. From the figures, if  $q$  increases, a gap of the dispersion is expanded. If  $q = 0$ , there is no corrugation but the plane wall which is the uniform structure indicated as periodic structure in section 2.2, so there are no gaps between the dispersion as shown in fig.2.2. Our approximate analytical solutions are limited by the value of  $q$ . We can find a good approximation when  $q$  is small (the smooth corrugation). In contrast, when  $q$  is large ( $> 0.1$ ) e.g., the structure of RF cavity, we can no longer use our approximation 2.15 and 2.16 in this case.

In addition in fig.2.5, with the fixed value of  $q$ , we vary a normalized cut-off angular frequencies  $\hat{\omega}_c$ . When  $\hat{\omega}_c$  increases the lowest angular frequency of electromagnetic waves which are allowed to propagate in a waveguide increases as well.

2.4. SOLUTION OF MATHIEU EQUATION: FLOQUET'S THEOREM

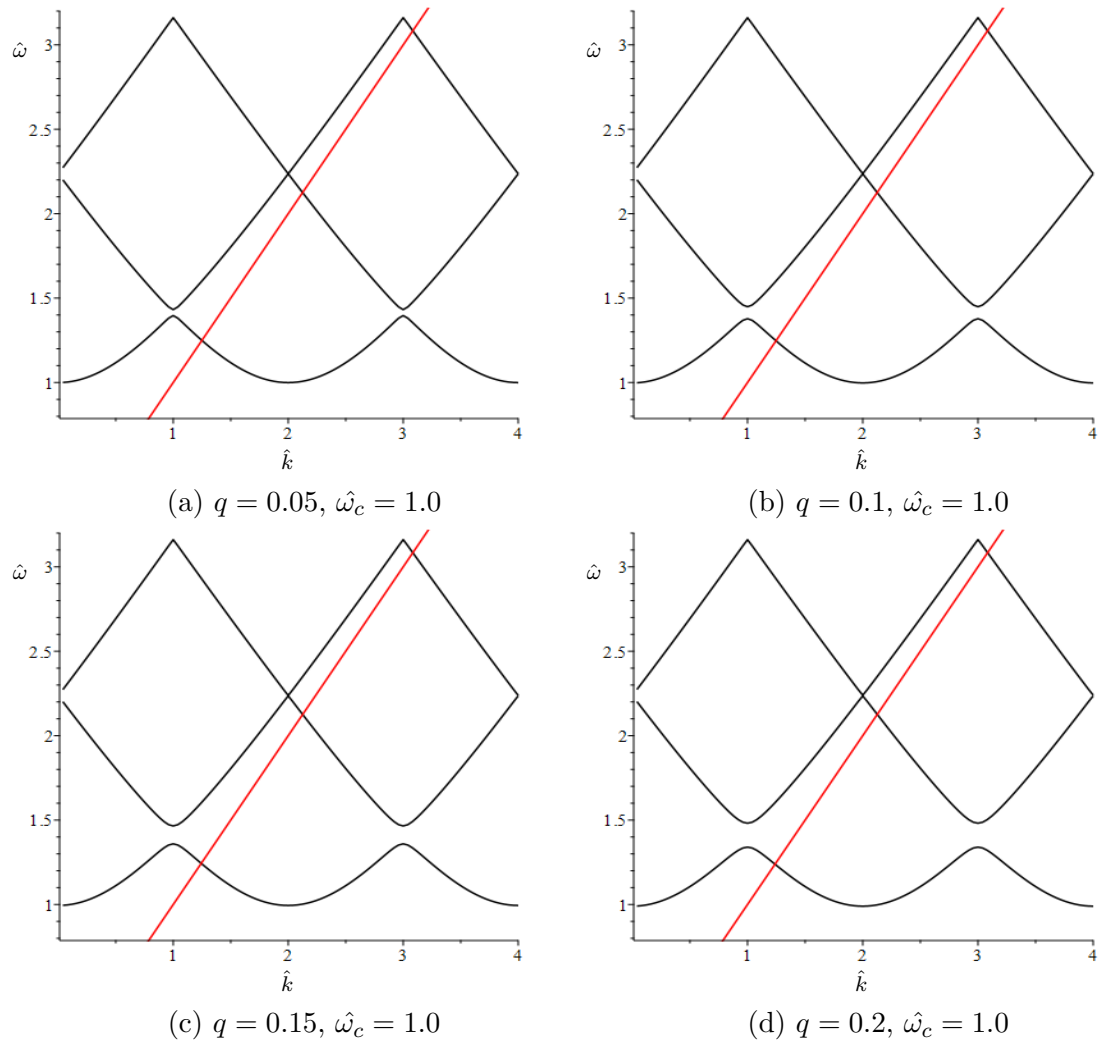


Figure 2.4: Reproduced figure from [16]. The dispersion relation with the fixed  $\omega_c$  and varying  $q$ . The red line is  $\hat{\omega} = \hat{k}$  and equals to the light line.

2.4. SOLUTION OF MATHIEU EQUATION: FLOQUET'S THEOREM

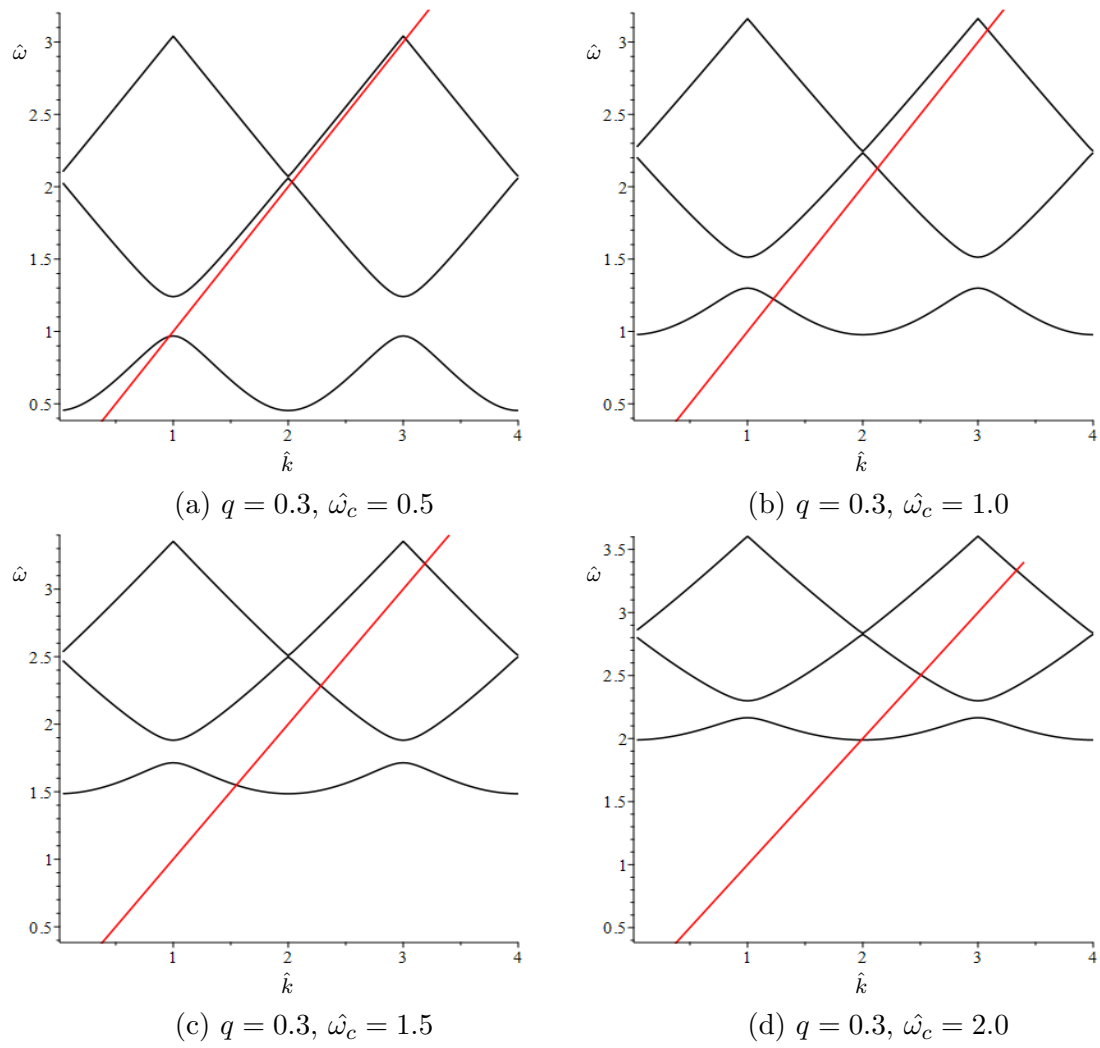


Figure 2.5: Reproduced figure from [16]. The dispersion relation with the fixed  $q$  and varying  $\omega_c$ . The red line is  $\hat{\omega} = \hat{k}$  and equals to the light line.

## 2.5 Dispersion Relation and CIP

The values of parameters  $\hat{\omega}$ ,  $\hat{\omega}_c$  and  $\hat{k}$  depend on the structures we considered, the (TM<sub>11</sub> mode) rectangular corrugated waveguide or the (TM<sub>01</sub> mode) cylindrical corrugated waveguide.

Parameters	Rectangular corrugated	Cylindrical corrugated
$\hat{\omega}$	$(L_z \omega)/(\pi c)$	$(L_z \omega)/(\pi c)$
$\hat{k}$	$(L_z k)/\pi$	$(L_z k)/\pi$
$\hat{\omega}_c$	$(L_z^2/L_0^2 + L_z^2/L_y^2)^{1/2}$	$(\chi_0^1 L_z)/(\pi R_0)$

In this research, we impose  $q = 0.1$ , because of a good agreement between analytical and numerical results of longitudinal electric fields that it can provide (section 3.2 and 5.2). When  $q = 0.1$ , the value of  $\hat{\omega}_c$  which there will be the CIP is 1.254. For the rectangular corrugated waveguide  $\hat{\omega}_c = (L_z^2/L_0^2 + L_z^2/L_y^2)^{1/2} = 1.254$ , we can choose the width  $L_y = 0.55$  mm, the length of a period  $L_z = 0.464$  mm, and the average height  $L_0 = 0.5$  mm. For the cylindrical corrugated waveguide  $\hat{\omega}_c = (\chi_0^1 L_z)/(\pi R_0) \approx 1.254$ , then the length of a period  $L_z = 0.59$  mm, and the average radius  $R_0 = 0.36$  mm. With these geometry parameters, the dispersion relation of  $q = 0.1$ , and  $\hat{\omega}_c = 1.254$  is shown in fig.2.6.

As previously introduced in section 1.3, the dispersion relation in fig.2.6 shows the relation between normalized angular frequencies  $\hat{\omega}$  and normalized wavenumbers  $\hat{k}$  of the symmetric corrugated waveguide  $q = 0.1$  and  $\hat{\omega}_c = 1.254$ . With this particular value of geometric parameters, particles with velocity  $\beta_e = 0.53$  (92 KeV) would be allowed to phase-synchronize with electric fields at  $\hat{k} = 2.857$  and  $\hat{\omega} = 1.513$  (for the rectangular corrugated waveguide  $f = 488.764$  GHz, and for the cylindrical corrugated waveguide  $f = 384.464$  GHz). Therefore, for the structures which have  $q = 0.1$ ,  $\hat{\omega}_c = 1.254$ , the CIP is  $\hat{\omega} = 1.513$ , and  $\hat{k} = 2.857$ .

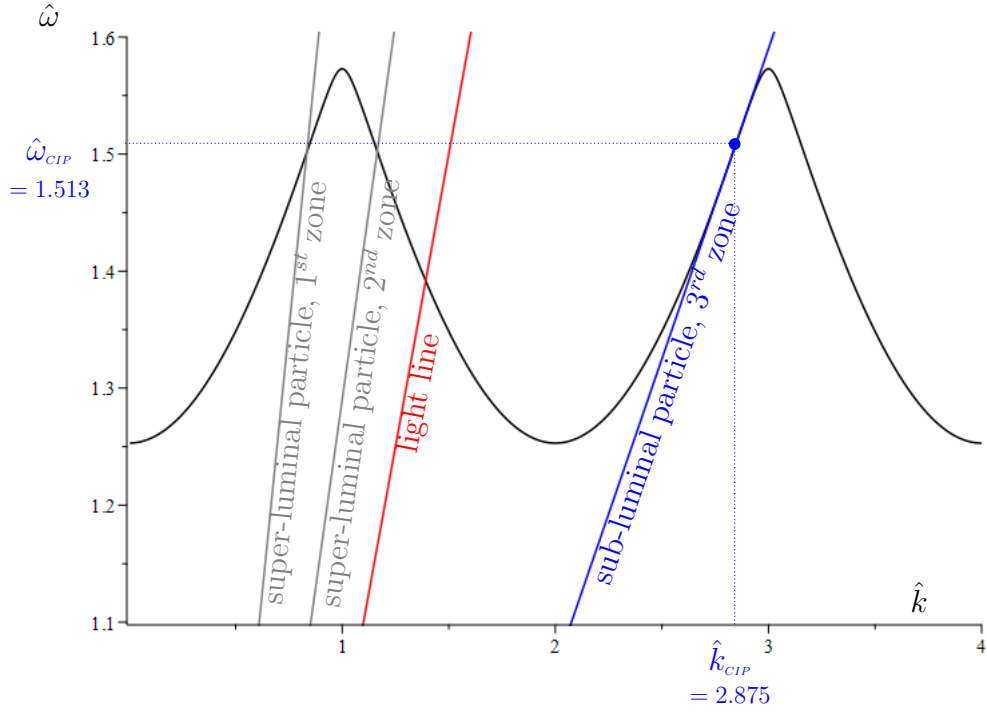


Figure 2.6: Reproduced figure from [16]. The dispersion relation of the rectangular corrugated waveguide with parameters  $q = 0.1$  and  $\omega_c = 1.254$ . A red line is the velocity of light. Gray lines and a blue line represent particle beam velocities that would interact with an electromagnetic wave: the first zone where a particle beam velocity is  $1.8c$ , the second zone where a particle beam velocity is  $1.29c$ , and the third zone is where a particle beam velocity is  $\beta_0 = 0.53$  (92 KeV).

By varying values of  $\hat{\omega}_c$ , and  $\hat{k}$  for each  $q$  in the determinant of matrix eq.2.24, we can solve the determinant for each set these values in Maple software. As a result, we found the particular set of  $\hat{\omega}_c$ ,  $\hat{k}_{CIP}$ , and  $\beta_e$  for each  $q$  that can satisfy 3 conditions for the CIP in section 1.3. We observed a parameter  $q$  from 0.00 to 0.30, the CIP only exists when  $\hat{\omega}_c$  correspond to  $q$  as shown in table 2.1 and fig.2.7. In addition, the velocity of a particle that would interact with an electric field runs from  $0.47c$  to  $0.56c$  as shown in fig.2.7b.

$q$	$\hat{\omega}_c$	$\hat{k}_{CIP}$	$\beta_e$
0.01	1.379	2.967	0.568
0.05	1.312	2.907	0.548
0.1	1.254	2.857	0.53
0.15	1.208	2.818	0.514
0.2	1.168	2.785	0.499
0.25	1.134	2.757	0.485
0.3	1.104	2.732	0.472

Table 2.1: The table selected sample of  $q$ , and  $\hat{\omega}_c$  and their CIP.

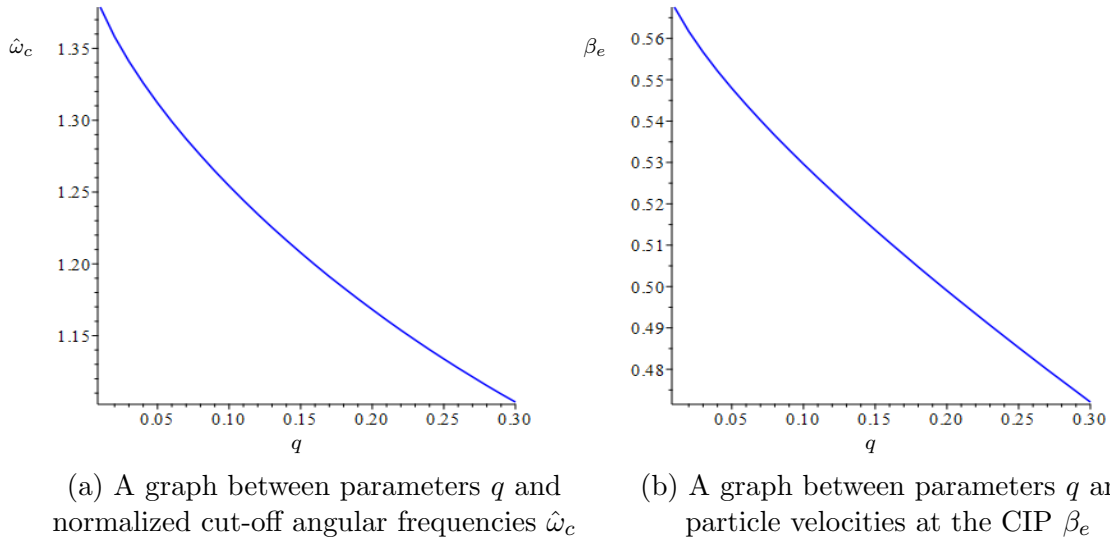


Figure 2.7: Reproduced figure from [16]. The relation between  $q$  and  $\hat{\omega}_c$ , and  $q$  and  $\beta_e$  determine that with these values there will be the CIP.

Nevertheless, because the CIP only exists for particular group of parameters ( $q$ ,  $\hat{\omega}_c$ , and  $\hat{k}_{CIP}$ ), this leads to the limitation that only a particle travels with the specific velocity ( $\beta_e$  corresponds to each  $q$  in table 2.1) would synchronize with a phase velocity of an electric field.

## 2.6 Particle-Field Interaction of Corrugated Waveguides

From the magnetic field of the symmetric corrugated waveguide in eq.2.15 and eq.2.16, the longitudinal electric fields  $TM_{11}$  at the center  $x = 0$ ,  $y = 0$  of the rectangular corrugated waveguide is

$$\mathbf{E}_{z(rec)} = B_0(\kappa_x^2(z) + \kappa_y^2)\phi(\eta z)\mathbf{e}_z \quad (2.25)$$

and the longitudinal electric fields  $TM_{01}$  at the center  $r = 0$  of the cylindrical corrugated waveguide is

$$\mathbf{E}_{z(cyl)} = B_0g(\eta z)\phi(\eta z)J_0(0)\mathbf{e}_z \quad (2.26)$$

we will show that there is an exchange of energy between particles and electric field for these structures.

Let us consider the electric field in time domain of the rectangular corrugated waveguide eq.2.25 is

$$\begin{aligned} \mathbf{E}(t, z) &= \frac{1}{2\pi}B_0(\kappa_x^2(z) + \kappa_y^2)\text{Re}\left[\int \phi(\eta z)e^{-i\omega t}\rho(\omega)d\omega\right] \\ &= \frac{1}{2\pi}B_0(\kappa_x^2(z) + \kappa_y^2)\text{Re}\left[\int e^{i\hat{k}z}\Psi_{a,q,\hat{k}}(\pi L_z^{-1}z)e^{-i\omega t}\rho(\omega)d\omega\right] \end{aligned} \quad (2.27)$$

after time pass  $t_p = t_0 + \frac{z_p}{c\beta_e}$  the electric field is

$$\mathbf{E}(t_p, z_p) = \frac{1}{2\pi}B_0(\kappa_x^2(z_p) + \kappa_y^2)\text{Re}\left[\int e^{i\hat{k}z_p}\Psi_{a,q,\hat{k}}(\pi L_z^{-1}z_p)e^{-i\omega(t_0+z_p/c\beta_e)}\rho(\omega)d\omega\right] \quad (2.28)$$

because  $\rho(\omega) = \delta(\omega - \omega_s)$ , then

$$\mathbf{E}(t_p, z_p) = \frac{1}{2\pi} B_0 (\kappa_x^2(z_p) + \kappa_y^2) \text{Re} \left[ \Psi_{a,q,\hat{k}}(\pi L_z^{-1} z_p) \right] \cos(\omega_s t_0) \quad (2.29)$$

substitute  $\kappa_x = \pi(L_0^{-2} + 2L_z^{-2}q \cos 2\pi L_z^{-1}z)^{1/2}$  and  $\kappa_y = \pi L_y^{-1}$  in eq.2.29

$$\mathbf{E}(t_p, z_p) = \pi B_0 L_z^{-2} (\hat{\omega}_c^2 + 2q \cos(2\pi L_z^{-1} z_p)) \text{Re} \left[ \Psi_{a,q,\hat{k}}(\pi L_z^{-1} z_p) \right] \cos(\omega_s t_0) \quad (2.30)$$

The integrated of an electric force, the total change in energy ( $\Delta e_p$ ) of a particle traveling over a period of structure  $L_z$  is

$$\begin{aligned} \Delta e_p &= q \int_0^{L_z} \mathbf{E}(t_p, z_p) dz_p \\ &= q\pi B_0 L_z^{-2} \cos(\omega_s t_0) \int_0^{L_z} (\hat{\omega}_c^2 + 2q \cos(2\pi L_z^{-1} z_p)) \text{Re} \left[ \Psi_{a,q,\hat{k}}(\pi L_z^{-1} z_p) \right] dz_p \end{aligned} \quad (2.31)$$

The fig.2.8 is the graph from eq.2.31 between the force which is felt by particles and the traveling distance. The graph shows that all the zones of different  $\hat{k}$ , the total force that a particle experiences (the total change in energy ( $\Delta e_p$ )) is not equal to 0. This means there is an energy exchange between a particle and an electric field.

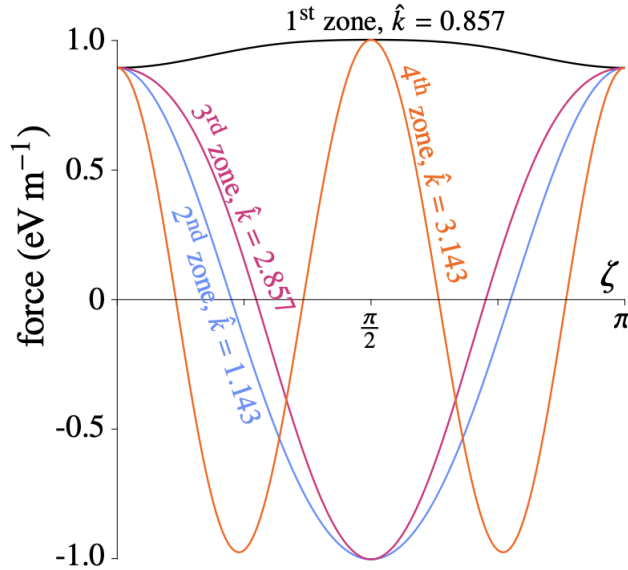


Figure 2.8: The figure from [16]. The graph between the force which is felt by particles in the rectangular corrugated waveguide with  $q = 0.1$  and  $\hat{\omega}_c = 1.255$ . The amplitude of an electric field is  $1\text{Vm}^{-1}$ . We determine 4 zones, the first zone (black) is the super-luminal particle where  $\hat{k} = 0.857$ ,  $\beta_e = 1.766$ , total force  $\Delta e_p = 4.81$ . The second zone (blue) is also the super-luminal particle,  $\hat{k} = 1.143$ ,  $\beta_e = 1.143$ ,  $\Delta e_p = -0.516$ . The third zone (red) is the sub-luminal particle,  $\hat{k} = 2.857$ ,  $\beta_e = 0.53$ , where is the CIP of this structure, the total force is  $\Delta e_p = 0.244$ . The sub-luminal particle fourth zone (orange),  $\hat{k} = 3.142$ ,  $\beta_e = 0.481$ , total force  $\Delta e_p = -0.043$ .

We show that there is the change in the energy of a particle traveling along a corrugated waveguide (the rectangular corrugated waveguide [16]) as shown in

fig.2.9. The average energy of a particle that travels across the rectangular corrugated waveguide decreases and transfers to an electric field. This enhances an amplitude of an electromagnetic wave. So, by using the corrugated waveguide in TWTs, we can amplify RF signals.

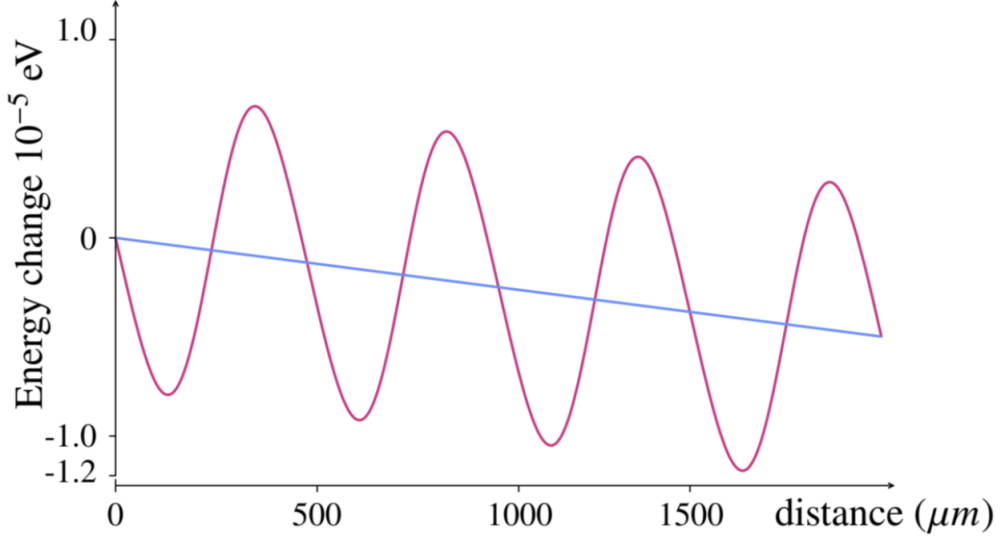


Figure 2.9: The figure from [16]. The graph between the change in the kinetic energy of a synchronous electron, from 92KeV ( $\beta_0 = 0.53$ , in the third zone which is the sub-luminal particle) in an RF field of  $1\text{Vm}^{-1}$ , and the traveling distance in the rectangular corrugated waveguide with  $q = 0.1$  and  $\hat{\omega}_c = 1.255$ . The blue line is the average of energy loss.

Similar to the cylindrical corrugated waveguide, the electric field in time domain is

$$\mathbf{E}(t_p, z_p) = \frac{1}{2\pi} B_0 J_0(0) g(\pi L_z^{-1} z_p) \text{Re} \left[ \Psi_{a,q,\hat{k}}(\pi L_z^{-1} z_p) \right] \cos(\omega_s t_0) \quad (2.32)$$

where  $g(\pi L_z^{-1} z_p) = \pi \left( (\chi_0^1)^2 \pi^{-2} R_0^{-2} + 2L_z^{-2} q \cos(2\pi L_z^{-1} z_p) \right)^{1/2}$ , the total change in energy of a particle is

$$\Delta e_p = q\pi B_0 J_0(0) \cos(\omega_s t_0) \int_0^{L_z} \left( (\chi_0^1)^2 \pi^{-2} R_0^{-2} + 2L_z^{-2} q \cos(2\pi L_z^{-1} z_p) \right)^{1/2} \text{Re} \left[ \Psi_{a,q,\hat{k}}(\pi L_z^{-1} z_p) \right] dz_p \quad (2.33)$$

The total change in the energy of a particle is not equal to 0 in the cylindrical corrugated waveguide.

Therefore, the symmetric corrugated waveguides both the rectangular and the cylindrical corrugated waveguide allow particles and electric field to exchange the energy, we can amplify the amplitude of RF signals by using our structure in TWTs.

## 2.7 Summary of a chapter 2

In section 2.1 to 2.3, we shows that there is no interaction between a particle and an electric field in a uniform waveguide (the total change in energy is equal 0) because a phase velocity is greater than the velocity of light. However, this problem can be solved by using the periodic structure instead of a uniform structure as shown in fig.2.3 where a phase velocity is less than the velocity of light and a particle can exchange the energy with an electric field (section 2.6).

For our structure, the symmetric corrugated waveguide, in section 2.4, we introduce Mathieu parameters,  $q$  which is a depth of the corrugation, parameter  $a$  which is equal to  $\hat{\omega}^2 - \hat{\omega}_c^2$  ( $\hat{\omega}$  is a normalized angular frequency and  $\hat{\omega}_c$  is a normalized cut-off angular frequency). We apply Floquet's theorem to solve Mathieu equation, then we get the relation between  $q$  and  $a = \hat{\omega}^2 - \hat{\omega}_c^2$  from the determinant in eq.2.24. From this determinant, we can plot the dispersion relation  $\hat{\omega} - \hat{k}$  ( $\hat{k}$  is a normalized wavenumber), and can design our structure by considering these parameters. For example, in chapter 4 the dispersion relation parameters of  $TM_{01}$  mode for the cylindrical corrugated waveguide structure are  $\hat{\omega} = (L_z \omega)/(\pi c)$ ,  $\hat{k} = (L_z k)/\pi$ ,  $\hat{\omega}_c = \chi_0^1 L_z / \pi R_0$  where  $L_z$  is the length of a period of the corrugation,  $R_0$  is an average radius of the waveguide. We define  $q = 0.1$ ,  $R_0 = 0.36$  mm,  $L_z = 0.59$  mm, then  $\hat{\omega}_c \approx 1.254$ . From these parameters, our waveguide allows the electromagnetic wave at frequency above 318.09 GHz (determine from  $\hat{\omega} = 1.252$  at  $\hat{k} = 0$ ) to pass through the structure.

In addition, in section 2.5, we found the CIP of each parameter  $q$  as shown in table 2.1. The table shows that the CIP can be found only if we design our structure  $\hat{\omega}_c$  corresponding to the value of  $q$ . This means if we use  $q = 0.1$ , we need to design the structure that has  $\hat{\omega}_c = 1.254$ , and there will be the CIP for this structure that particles would interact with the wide range frequencies of an electric field with the particular synchronous phase velocity  $\beta_e = 0.53$  (92 KeV). However, due to the CIP only exists for particular group of parameters ( $q$ ,  $\hat{\omega}_c$ , and  $\hat{k}_{CIP}$  as shown in table 2.7), this means the particle with only specific velocity ( $\beta_e$ ) will synchronize with a phase velocity of an electric field. Therefore, to enhance the interaction between particles and an electric field, we need to chose the velocity of particles corresponding to the CIP of the structure.

# Chapter 3

## Rectangular Corrugated Waveguide

### 3.1 Electric Field and Magnetic Field

The rectangular corrugated waveguide has a slow-wave profile as shown in fig.3.1,

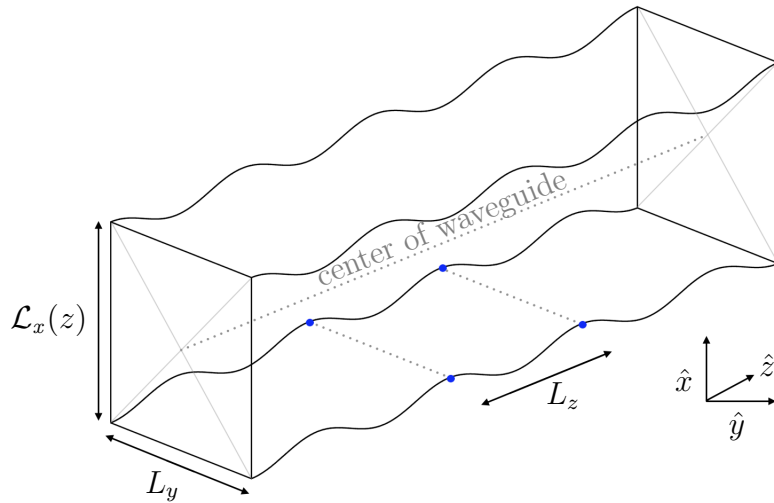


Figure 3.1: The rectangular corrugated waveguide profile.

The waveguide's height  $\mathcal{L}_x(z)$  depends on  $z$ , because of the corrugation. This  $\mathcal{L}_x(z)$  oscillates around an average value, we define this value as  $L_0$ . The width is represented by  $L_y$ . The length of each corrugation is  $L_z$ . Both parameters are fixed.

Because our solutions for an electromagnetic field are an approximation, there are errors needed to consider, we expressed these errors in Maxwell's equations

$$\begin{aligned} \nabla \cdot \tilde{\mathbf{E}} &= 0 & \nabla \times \tilde{\mathbf{E}} - i\omega \tilde{\mathbf{B}} &= \varepsilon_{Max} \\ \nabla \cdot \tilde{\mathbf{B}} &= 0 & \nabla \times \tilde{\mathbf{B}} + i\omega c^{-2} \tilde{\mathbf{E}} &= 0 \end{aligned} \quad (3.1)$$

and in the boundary conditions

$$\tilde{\mathbf{E}}_{\parallel}|_{Bdd} = \varepsilon_{Bdd} \quad \tilde{\mathbf{B}}_{\perp}|_{Bdd} = 0 \quad (3.2)$$

Because there are errors ( $\epsilon_{Max}$  and  $\epsilon_{Bdd}$ ) occurring, the solution which is solved from these Maxwell's equations will be an approximation.

To allow a particle and an electric field interact, we chose TM mode of an electromagnetic field. Since there is only the electric field at the center of the waveguide where a particle is accelerated. For the TM mode magnetic field is

$$\begin{aligned} \tilde{\mathbf{B}} = B_0 c^{-2} (-i\omega) \phi(\eta z) & \left( \kappa_y \cos(\kappa_x x) \sin(\kappa_y y) \mathbf{e}_x \right. \\ & \left. - \kappa_x \sin(\kappa_x x) \cos(\kappa_y y) \mathbf{e}_y \right) \end{aligned} \quad (3.3)$$

and the electric field is

$$\begin{aligned} \tilde{\mathbf{E}} = B_0 & \left( (\kappa'_x \sin(\kappa_x x) + \kappa'_x \kappa_x x \cos(\kappa_x x) + \eta \kappa_x \sin(\kappa x) \phi'(\eta z)) \phi(\eta z) \right) \cos(\kappa_y y) \mathbf{e}_x \\ & + B_0 \kappa_y \left( -\kappa'_x x \sin(\kappa_x x) \phi(\eta z) + \eta \cos(\kappa_x x) \phi'(\eta z) \right) \sin(\kappa_y y) \mathbf{e}_y \\ & - B_0 (\kappa_x^2 + \kappa_y^2) \cos(\kappa_x x) \cos(\kappa_y y) \phi(\eta z) \mathbf{e}_z. \end{aligned} \quad (3.4)$$

with parameters  $\kappa_x(z)$ ,  $\kappa_y$ , and  $\eta$  as defined by the following equations

$$\kappa_x(z) = \frac{\pi p_x}{\mathcal{L}_x(z)} \quad \kappa_y = \frac{\pi p_y}{L_y} \quad \eta = \frac{\pi}{L_z} \quad (3.5)$$

We introduce a function  $\phi(\eta z)$  which has the role to adjust the electromagnetic field according to the corrugated wall, by substituting  $\tilde{\mathbf{B}}$  and  $\tilde{\mathbf{E}}$  into Faraday's law eq.3.1 gives the 2nd order ODE of  $\phi(\zeta)$

$$\phi''(\zeta) + \eta^{-2} \left( c^{-2} \omega^2 - \kappa_x^2 - \kappa_y^2 \right) \phi(\zeta) = 0 \quad (3.6)$$

where  $\zeta = \eta z$  is dimensionless parameter. The eq.3.6 can be rewritten in the form of Mathieu equation

$$\phi''(\zeta) + \left( a - 2q \cos(2\zeta) \right) \phi(\zeta) = 0 \quad (3.7)$$

By comparing eq.3.6 and eq.3.7, we get parameters of the rectangular corrugated waveguide ( $\mathcal{L}_x(z)$ ,  $L_0$ ,  $L_y$ , and  $L_z$ ) in the term of Mathieu equation variables ( $q$  and  $a$ )

$$\begin{aligned} a - 2q \cos(2\zeta) & \equiv \eta^{-2} \left( c^{-2} \omega^2 - \kappa_x^2 - \kappa_y^2 \right) \\ & = L_z^2 \left( c^{-2} \pi^{-2} \omega^2 - p_x^2 \mathcal{L}_x(z)^{-2} - p_y^2 L_y^{-2} \right) \\ & = L_z^2 \left( c^{-2} \pi^{-2} \omega^2 - p_x^2 L_0^{-2} - p_y^2 L_y^{-2} \right) - L_z^2 \left( p_x^2 \mathcal{L}_x(z)^{-2} - p_x^2 L_0^{-2} \right) \end{aligned} \quad (3.8)$$

From eq.3.8, the first term of Mathieu equation, parameter  $a$  is

$$a = L_z^2 \left( c^{-2} \pi^{-2} \omega^2 - p_x^2 L_0^{-2} - p_y^2 L_y^{-2} \right) \quad (3.9)$$

to simplify eq.3.9, we define 2 dimensionless variables, a normalized angular frequency  $\hat{\omega}$  is a variable depends on angular frequency of the electromagnetic wave propagating through the waveguide, and a normalized wavenumber  $\hat{\omega}_c$  is a cut-off angular frequency depends on a geometry of the structure.

$$a = \hat{\omega}^2 - \hat{\omega}_c^2 \quad (3.10)$$

where

$$\hat{\omega} = \frac{L_z}{\pi c} \omega \quad \text{and} \quad \hat{\omega}_c = \left( \frac{L_z^2}{L_0^2} + \frac{L_z^2}{L_y^2} \right)^{1/2} \quad (3.11)$$

The second term of eq.3.8 is

$$2q \cos(2\zeta) = L_z^2 \left( p_x^2 \mathcal{L}_x(z)^{-2} - p_x^2 L_0^{-2} \right) \quad (3.12)$$

this yields the relation between Mathieu's parameter  $q$  and the function  $\mathcal{L}_x(\zeta)$  which can be used to design the profile of corrugations

$$\mathcal{L}_x(\zeta) = \left( L_0^{-2} + 2L_z^{-2} p_x^{-2} q \cos(2\zeta) \right)^{-\frac{1}{2}} \quad (3.13)$$

To get a good approximation of solutions,  $q$  and  $\delta = L_0/L_z$  need to be small (this approximation will be discussed in detail in chapter4. We can make an assumption that  $qL_0^2L_z^{-2}$  is small, the simplified form of  $\mathcal{L}_x(\zeta)$  is

$$\mathcal{L}_x(\zeta) \approx L_0^{-2} - L_0^3 L_z^{-2} p_x^{-2} q \cos(2\zeta) \quad (3.14)$$

From eq.3.14 and fig.3.2,  $L_0$  is the average height of the structure and a parameter  $q$  can be interpreted as the depth of the corrugations. If  $q$  is small, the depth of corrugations are small or smooth corrugation. On the other hand, the corrugations are getting deeper when  $q$  increases.

### 3.1. ELECTRIC FIELD AND MAGNETIC FIELD

---

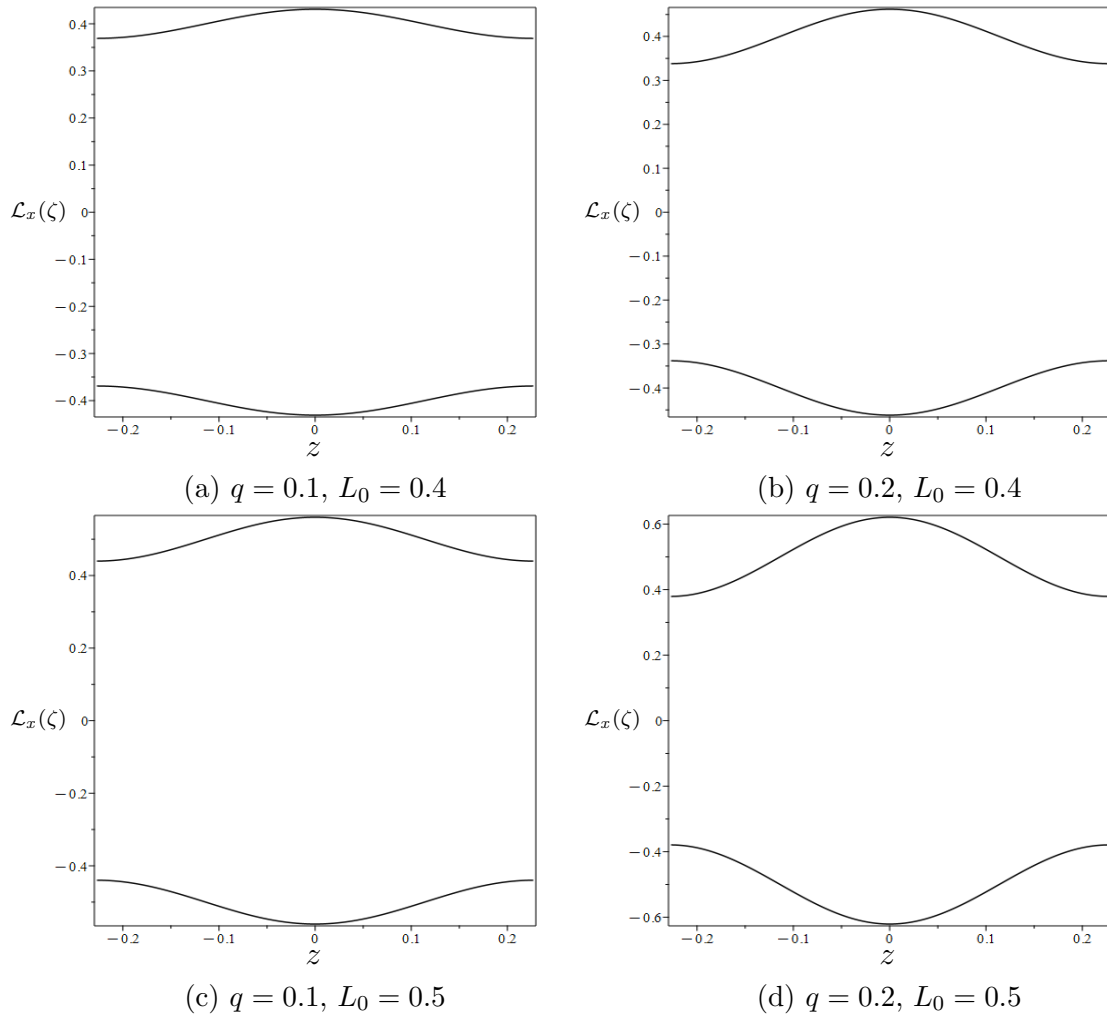


Figure 3.2: The rectangular corrugated profile with the variation in parameter  $q$  and  $L_0$ .

## 3.2 Numerical Solution of a Rectangular Corrugated Waveguide

To check the validity of the analytical solution that would predict particle-wave interaction, the commercial numerical simulation software CST is employed. CST is able to solve Maxwell integral equation on a tetrahedral mesh. The rectangular corrugated waveguide is designed with the boundary condition as perfect electric conductor (PEC) at all the walls. This makes a waveguide becomes resonator, therefore it is easier to determine the modes inside the structure because the amplitude of the electric field always starts at the entrance of the structure  $z = 0$  and ends at the end of the structures  $z = nL_z$ .

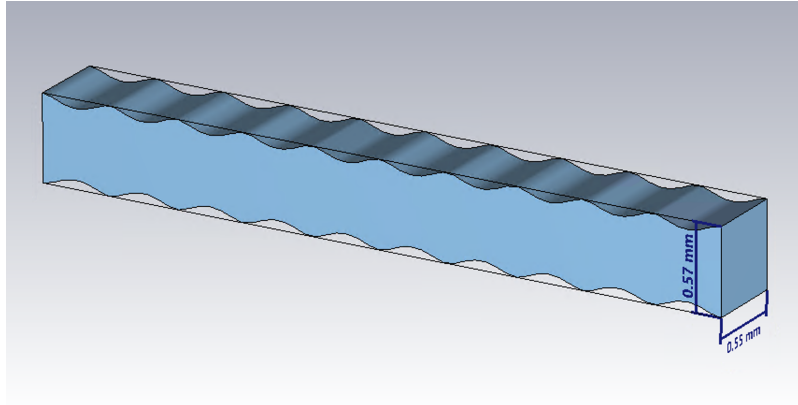


Figure 3.3: The rectangular corrugated waveguide profile with  $q = 0.1, L_y = 0.55$  mm  $L_0 = 0.5$  mm,  $L_z = 0.464$  mm,  $\omega_c = 1.254$  and 10 periods structure simulated by CST simulation (the reason that we use only 10 periods, because the software requires more time to process the results for the structure with more periods. For the future works, we will work on the corrugated waveguide with more periods, this will increase the accuracy of finding a phase and a group velocity of CST results fig.3.6b).

The geometry of the rectangular corrugated waveguide that used to simulate the results in CST is  $q = 0.1, L_y = 0.55$  mm  $L_0 = 0.5$  mm,  $L_z = 0.464$  mm, and 10 periods structure. With this profile a normalize cut-off angular frequency is  $\hat{\omega}_c = 1.254$ , the CIP  $\hat{k}_{CIP} = 2.857$ ,  $\hat{\omega}_{CIP} = 1.513$  which are equivalent to  $k_{CIP} = 19.344$  mm<sup>-1</sup>,  $f_{CIP} = 488.764$  GHz and  $\beta_e = 0.53$ .

We examine the normalized longitudinal electric field  $E_z$  TM<sub>11</sub> mode along the center ( $x = 0, y = 0$ ) of the structure. By plotting the  $E_z$  vs  $z$  of the CST's exported data and the analytical results

$$\mathbf{E}_z = B_0(\kappa_x^2 + \kappa_y^2) \cos(\kappa_x x) \cos(\kappa_y y) \phi(\eta z) \mathbf{e}_z \quad (3.15)$$

we can compare the analytical and numerical results as shown in fig.3.4. Although they are not perfectly fit, overall the analytical graphs are match with the numerical field patterns with different  $\hat{k}$ .

### 3.2. NUMERICAL SOLUTION OF A RECTANGULAR CORRUGATED WAVEGUIDE

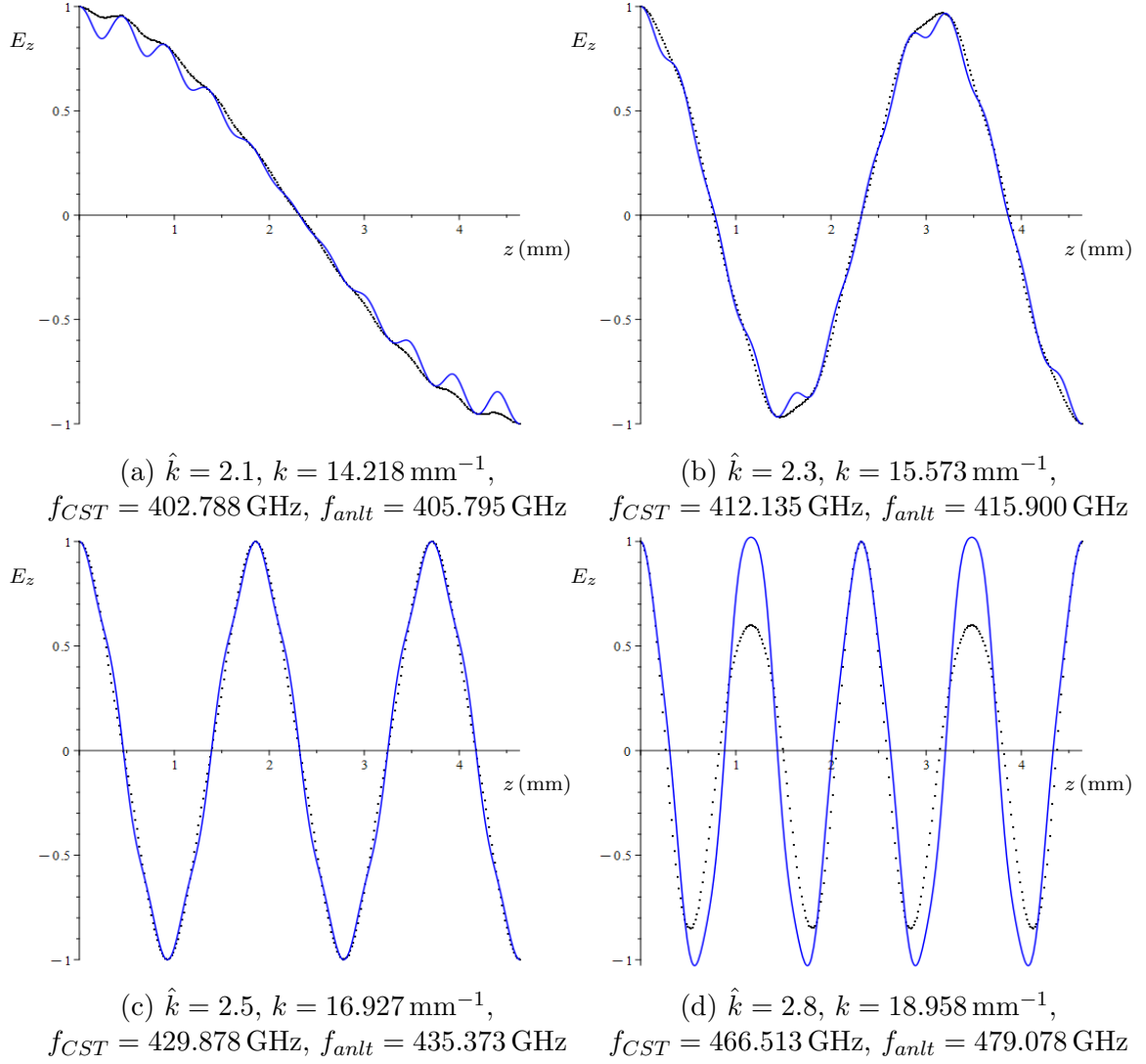


Figure 3.4: The electric field  $\text{TM}_{11}$  mode at the center  $x = 0$ ,  $y = 0$  of the rectangular corrugated waveguide  $q = 0.1$ ,  $L_y = 0.55 \text{ mm}$ ,  $L_0 = 0.5 \text{ mm}$ ,  $L_z = 0.464 \text{ mm}$ , 10 period structure,  $\hat{\omega}_c = 1.254$ , the CIP is  $\hat{k}_{CIP} = 2.857$ ,  $\hat{\omega}_{CIP} = 1.513$  which are equivalent to  $k_{CIP} = 19.344 \text{ mm}^{-1}$ ,  $f_{CIP} = 488.764 \text{ GHz}$  and  $\beta_e = 0.53$ .

### 3.2. NUMERICAL SOLUTION OF A RECTANGULAR CORRUGATED WAVEGUIDE

We collect the frequencies of  $\hat{k}$  values from CST simulation, plot and compare them with the analytical frequencies, the dispersion relation between analytical and numerical results is shown in fig.3.5.

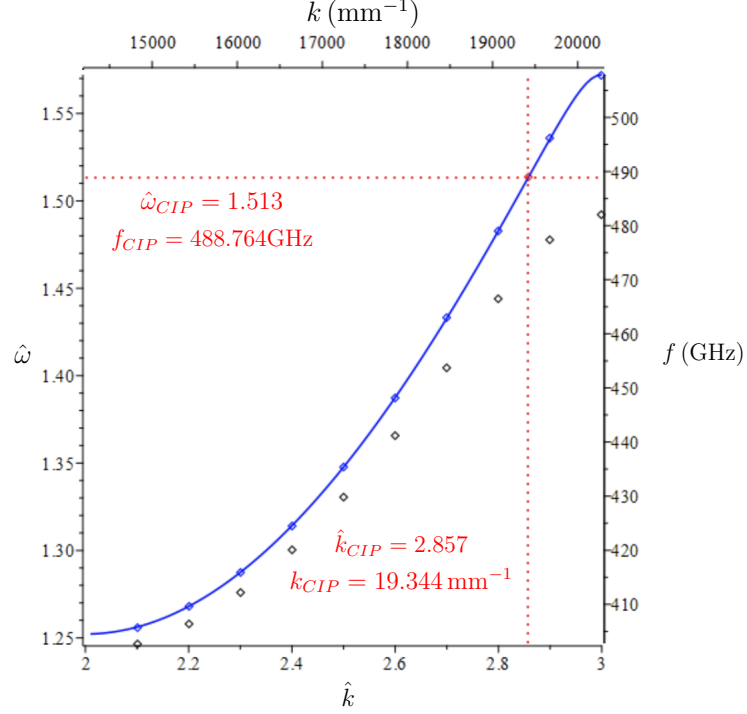


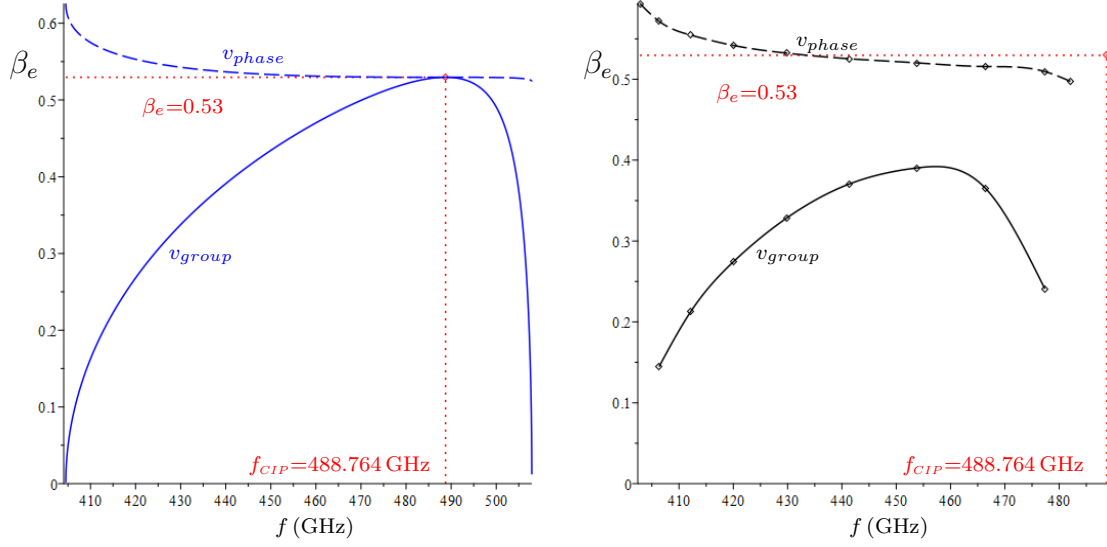
Figure 3.5: The dispersion relation result from CST (black dots) and analytical equation (blue line and blue dots) of the rectangular corrugated waveguide  $q = 0.1$ ,  $L_y = 0.55$  mm,  $L_0 = 0.5$  mm,  $L_z = 0.464$  mm, 10 period structure,  $\hat{\omega}_c = 1.254$ , and the CIP is  $\hat{k}_{CIP} = 2.857$ ,  $\hat{\omega}_{CIP} = 1.513$  which are equivalent to  $k_{CIP} = 19.344$  mm $^{-1}$ ,  $f_{CIP} = 488.764$  GHz and  $\beta_e = 0.53$ .

From our analytical solution we expect to see the CIP of structure  $q = 0$  and  $\hat{\omega}_c = 1.254$  (which the geometry parameters of the rectangular corrugated waveguide are  $L_y = 0.55$  mm,  $L_0 = 0.5$  mm,  $L_z = 0.464$  mm) at  $k_{CIP} = 19.344$  mm $^{-1}$ ,  $f_{CIP} = 488.764$  GHz. We can observe whether there is the CIP for our structure, by examine phase and group velocities graph.

Fig.3.6 presents phase and group velocities of analytical (3.6a) and numerical (3.6b) results of the structure  $q = 0.1$  and  $\hat{\omega}_c = 1.254$ . For analytical results, there is the CIP at  $f_{CIP} = 488.764$  GHz and  $\beta_e = 0.53$  exactly the same point which predicted by the mathematic model.

On the other hand, from the works by [16], we found that for numerical results, the CIP for  $q = 0.1$  is available when  $\hat{\omega}_c = 1.06$  (for structure  $L_y = 1$  mm,  $L_0 = 0.41$  mm, and  $L_z = 0.475$  mm) as appearing in fig.3.7. Where the CIP is  $f_{CIP} = 394$  GHz and  $\beta_e = 0.46$ .

### 3.2. NUMERICAL SOLUTION OF A RECTANGULAR CORRUGATED WAVEGUIDE



(a) Phase and group velocity of analytical results (b) Phase and group velocity of numerical (CST) results

Figure 3.6: Phase (dash line) and group (solid line) velocities of analytical results (blue) and numerical results (black) of the rectangular corrugated waveguide  $q = 0.1$ ,  $L_y = 0.55$  mm,  $L_0 = 0.5$  mm,  $L_z = 0.464$  mm, 10 period structure  $n = 10$ ,  $\hat{\omega}_c = 1.254$ , and the CIP of analytical solution is  $\hat{k}_{CIP} = 2.857$ ,  $\hat{\omega}_{CIP} = 1.513$  which are equivalent to  $k_{CIP} = 19.344$  mm $^{-1}$ ,  $f_{CIP} = 488.764$  GHz and  $\beta_e = 0.53$  (92 KeV).

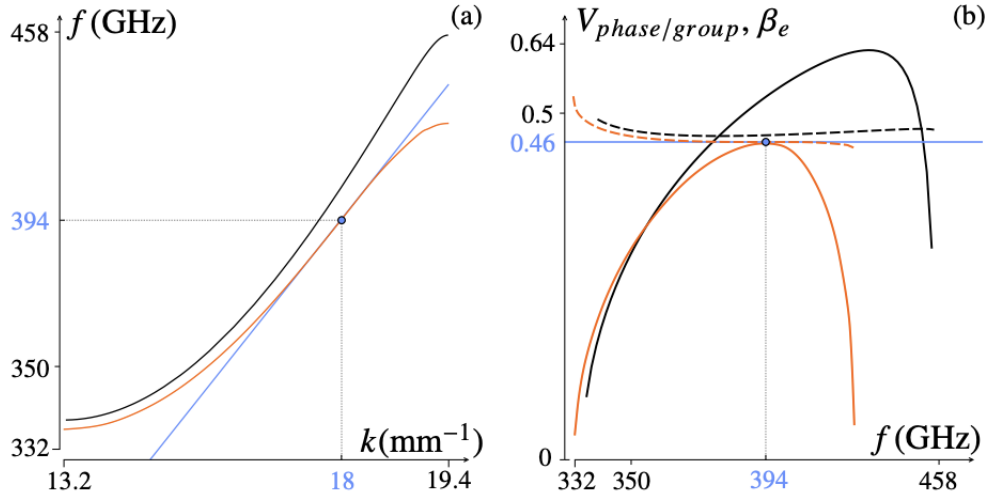


Figure 3.7: Figure from [16]. (a) The dispersion relation result from CST (orange) of structure  $\hat{\omega}_c = 1.06$  and analytical equation (black) of structure  $\hat{\omega}_c = 1.255$ . (b) Phase (dash line) and group (solid line) velocities of CST (orange) of structure  $\hat{\omega}_c = 1.06$  and analytical equation (black) of structure  $\hat{\omega}_c = 1.255$ . Where the CIP of numerical results is  $f_{CIP} = 394$  GHz and  $\beta_e = 0.46$  (65 KeV).

### 3.3 Summary of a chapter 3

In section 3.1, we show that with the modified Maxwell's equation eq.3.1 and the boundary conditions eq.3.2, we can find the analytical results of the  $TM_{11}$  magnetic field eq.3.3, and the electric field eq.3.4. We introduce  $\phi(\eta z)$  to be a function for adjusting the electromagnetic fields due to the corrugated wall. Because  $\phi(\eta z)$  can be solved by Mathieu equation, we rewrite parameters of the waveguide in the form of Mathieu equation. Therefore parameters for the rectangular corrugated waveguide are  $\hat{\omega} = (L_z \omega)/(\pi c)$ ,  $\hat{k} = (L_z k)/\pi$ , and  $\hat{\omega}_c = (L_z^2/L_0^2 + L_z^2/L_y^2)^{1/2}$ . In addition, we can define the waveguide's height from this rewritten parameters in the form of Mathieu equation as shown in eq.3.14, where  $L_0$  is the average height of the waveguide.

In section 3.2, a simulation software CST is utilized to solve Maxwell's equations of a rectangular corrugated waveguide. We design the structure which has  $q = 0.1$ ,  $L_y = 0.55$  mm,  $L_0 = 0.5$  mm,  $L_z = 0.464$  mm, and  $\hat{\omega}_c = 1.254$ , with these parameters the CIP of this structure is  $\hat{k}_{CIP} = 2.857$ ,  $\hat{\omega}_{CIP} = 1.513$ ,  $\beta_e = 0.53$  (92 KeV),  $f_{CIP} = 488.764$  GHz. We plot the normalized longitudinal electric field  $TM_{11}$  mode at the center of the waveguide  $E_z$  and  $z$ , and compare results from our analytical results with the CST results as shown in fig.3.4. The graph shows a good agreement between these two results. However, the CIP from analytical results is not the same point as the numerical results from CST. As shown in fig.3.6, and fig.3.7, the CIP of numerical results is the point where a phase velocity, a group velocity, and a particle velocity are coincided. Hence, for the rectangular corrugated waveguide  $q = 0.1$ , the CIP of numerical results exists for the structure  $L_y = 1$  mm,  $L_0 = 0.41$  mm,  $L_z = 0.475$  mm, and  $\hat{\omega}_c = 1.06$ . The CIP of this structure is  $f_{CIP} = 394$  GHz, and  $\beta_e = 0.46$  (65 KeV).

# Chapter 4

## Theory of the Cylindrical Corrugated Waveguide

### 4.1 Electric Field and Magnetic Field

The particles such as electrons can be accelerated by the electric field along the z-direction, so that the mode of waveguide will be Transverse Magnetic (TM) modes. To find the analytical solutions of the cylindrical corrugated waveguide, we will start with the 4 equations of Maxwell's in vacuum in the frequency domain

$$\nabla \cdot \tilde{\mathbf{E}} = 0 \quad (4.1)$$

$$\nabla \cdot \tilde{\mathbf{B}} = 0 \quad (4.2)$$

$$\nabla \times \tilde{\mathbf{E}} - i\omega\tilde{\mathbf{B}} = \varepsilon_{Max} \quad (4.3)$$

$$\nabla \times \tilde{\mathbf{B}} + i\omega c^{-2}\tilde{\mathbf{E}} = 0 \quad (4.4)$$

For a Faraday's law in eq.4.3, the right hand side of an equation is equal to the error ( $\varepsilon_{Max}$ ), due to the solution that we will find later is an approximation.

In addition, because the wall of the waveguide is the corrugation. This leads to the boundary condition of the electromagnetic field that is parallel to the wall of the waveguide is not equal to 0 but equal to an error at boundary ( $\varepsilon_{Bdd}$ ).

$$\begin{aligned} \tilde{\mathbf{E}}_{\parallel}|_{Bdd} &= \varepsilon_{Bdd} \\ \tilde{\mathbf{B}}_{\perp}|_{Bdd} &= 0 \end{aligned} \quad (4.5)$$

Regarding to a uniform cylindrical waveguide, the magnetic field along the waveguide in z-direction of TM modes are the Bessel functions of the first kind

$$\tilde{\mathbf{B}} = B_0 c^{-2} (-i\omega) J_1(rk_{\rho_{mn}}) \mathbf{e}_{\theta} \quad (4.6)$$

$k_{\rho_{mn}} = P_{mn}/R$ , where  $P_{mn}$  is the  $n^{th}$  root of  $J_m$ , and  $R$  is a radius of a uniform waveguide. Then we can modify it to the cylindrical corrugated waveguide model from eq.4.6

$$\tilde{\mathbf{B}} = B_0 c^{-2} (-i\omega) \phi(\eta z) J_1(rg(\eta z)) \mathbf{e}_{\theta} \quad (4.7)$$

$\phi(\eta z)$  is an additional function inserted into the magnetic field equation of a uniform waveguide. This  $\phi(\eta z)$  allows the magnetic field adjust itself along z-direction, because of the corrugated wall.

Substituting  $\tilde{\mathbf{B}}$  in eq. 4.4 to find the electric field  $\tilde{\mathbf{E}}$ , then

$$\begin{aligned} \tilde{\mathbf{E}} = & g^{-1} B_0 [-g' g r \phi(\eta z) J_0(r g) - g \eta \phi'(\eta z) J_1(r g) + g' \phi(\eta z) J_1(r g)] \mathbf{e}_r \\ & (0) \mathbf{e}_\theta + B_0 g \phi(\eta z) J_0(r g) \mathbf{e}_z \end{aligned} \quad (4.8)$$

Now we have the approximate results of the magnetic field and the electric field of the cylindrical waveguide. Next sections, we can find the values of  $\phi(\eta z)$  by minimizing an error max  $\varepsilon_{Max}$  and the solutions of Mathieu function.

## 4.2 The Error Max ( $\varepsilon_{Max}$ ) Minimization

The error ( $\varepsilon_{Max}$ ) of an approximation is a result of Faraday's law by substituting  $\tilde{\mathbf{E}}$  and  $\tilde{\mathbf{B}}$  in eq.4.3

$$\begin{aligned} \varepsilon_{Max} = & (0) \mathbf{e}_r - B_0 \{ [-g'' g^{-1} \phi + (-g'^2 r^2 + 2g'^2 g^{-2} - g^2 + c^{-2} \omega^2) \phi \\ & + \eta^2 \phi'' - \frac{g' g^{-2} \eta \phi}{2}] J_1 + [\frac{g' \eta \phi}{2} + g'' \eta - g'^2 g^{-2} \phi] r J_0 \} \mathbf{e}_\theta + (0) \mathbf{e}_z \end{aligned} \quad (4.9)$$

We consider smooth corrugation by letting  $g''$  and  $g'$  be very small. To obtain a good approximate result,  $\varepsilon_{Max}$  needs to be minimized, when

$$\phi''(\zeta) + \eta^{-2} (c^{-2} \omega^2 - g^2(\zeta)) \phi(\zeta) = 0 \quad (4.10)$$

( $\zeta$  is a scaled variable,  $\zeta := \frac{\pi z}{L_z} = \eta z$ ). Then  $\varepsilon_{Max}$  is

$$\begin{aligned} \varepsilon_{Max} = & (0) \mathbf{e}_r - B_0 \{ [-g'' g^{-1} \phi + (-g'^2 r^2 + 2g'^2 g^{-2}) \phi - \frac{g' g^{-2} \eta \phi}{2}] J_1 \\ & + [\frac{g' \eta \phi}{2} + g'' \eta - g'^2 g^{-2} \phi] r J_0 \} \mathbf{e}_\theta + (0) \mathbf{e}_z \end{aligned} \quad (4.11)$$

The corrugated structure causes errors to analytical solution. We group these errors into 2 groups, an  $\varepsilon_{Max}$  and an  $\varepsilon_{Bdd}$ . At the center of the structure,  $\varepsilon_{Max} = 0$ , this means there is no error causing by the corrugation, the error is gradually decreasing if we move from the center and end up be the most error at the wall of the structure. From the errors that we analyze, there are 2 constrains to be considered for designing the cylindrical corrugated structure.

1. The center of the cylindrical corrugated structure,  $\varepsilon_{Max}$  is equal to 0. We can exploit this advantage by injecting particles at the center.
2. Good approximation can be achieved by reducing the parameter  $q$ .

## 4.3 Boundary Conditions

At the boundary, the radius of the cylindrical corrugated waveguide ( $r$ ) varies along the structure, so  $r = R(z)$ . We can categorized vectors at the boundary into 2 vectors, a normal vector and a tangent vector.

1. normal vector  $(1 + R'(z)^2)^{-\frac{1}{2}}(\mathbf{e}_r - R'(z)\mathbf{e}_z)$ .
2. tangent vector  $\mathbf{e}_\theta$  and  $(1 + R'(z)^2)^{-\frac{1}{2}}(\mathbf{e}_z + R'(z)\mathbf{e}_r)$ .

Then, we can consider elements of the magnetic field  $\tilde{\mathbf{B}}$  and the electric field  $\tilde{\mathbf{E}}$  in a normal and a tangent vector.

A normal magnetic field at the boundary along the corrugations is

$$\tilde{\mathbf{B}}_\perp = \tilde{\mathbf{B}} \cdot (1 + R'(z)^2)^{-\frac{1}{2}}(\mathbf{e}_r - R'(z)\mathbf{e}_z) = 0B_0c^{-2}(-i\omega)\phi(\eta z)J_1(rg(\eta z))\mathbf{e}_\theta \quad (4.12)$$

and a tangent magnetic field is

$$\tilde{\mathbf{B}}_\parallel = \tilde{\mathbf{B}} \cdot (1 + R'(z)^2)^{-\frac{1}{2}}(\mathbf{e}_z + R'(z)\mathbf{e}_r) = 0 \quad (4.13)$$

A normal electric field at the boundary along the corrugations is

$$\begin{aligned} \tilde{\mathbf{E}}_\perp &= \tilde{\mathbf{E}} \cdot (1 + R'(z)^2)^{-\frac{1}{2}}(\mathbf{e}_r - R'(z)\mathbf{e}_z) \\ &= -B_0(1 + R'^2)^{\frac{1}{2}}g^{-1}[(g\eta\phi' - g'\phi)J_1 + (rg' + R'g)g\phi J_0]|_{r=R(z)} \end{aligned} \quad (4.14)$$

and from the boundary conditions in eq. 4.5

$$\begin{aligned} \tilde{\mathbf{E}}_\parallel &= \varepsilon_{Bdd} \\ &= \tilde{\mathbf{E}} \cdot (1 + R'(z)^2)^{-\frac{1}{2}}(\mathbf{e}_z + R'(z)\mathbf{e}_r) \\ &= -B_0(1 + R'^2)^{\frac{1}{2}}g^{-1}[R'(g\eta\phi' - g'\eta)J_1 + (rR'g' - g)g\phi J_0]|_{r=R(z)} \end{aligned} \quad (4.15)$$

## 4.4 Mathieu Equation of the Cylindrical Corrugated Waveguide

To complete the analytical solution, we have to find the value of  $\phi(\zeta)$ . We obtain the  $\phi(\zeta)$  from minimizing the  $\varepsilon_{Max}$ ,  $\phi''(\zeta) + \eta^{-2}(c^{-2}\omega^2 - g^2(\zeta))\phi(\zeta) = 0$ , This equation can be rewritten into formal Mathieu equation

$$\phi''(\zeta) + (a - 2q \cos(2\zeta))\phi(\zeta) = 0 \quad (4.16)$$

comparing eq.4.10 and eq.4.16, then

$$\begin{aligned} \phi''(\zeta) + (a - 2q \cos(2\zeta))\phi(\zeta) &= \phi''(\zeta) + \eta^{-2}(c^{-2}\omega^2 - g^2(z))\phi(\zeta) \\ a - 2q \cos(2\zeta) &= \eta^{-2}(c^{-2}\omega^2 - g(\zeta)^2) \\ &= L_z^2(c^{-2}\pi^{-2}\omega^2 - \pi^{-2}g(\zeta)^2) \end{aligned} \quad (4.17)$$

We introduce  $R_0$  as a physical parameter with a unit [m] into eq.4.17

$$\begin{aligned} a - 2q \cos(2\zeta) &= L_z^2(c^{-2}\pi^{-2}\omega^2 - (\chi_m^n)^2\pi^{-2}R_0^{-2} + (\chi_m^n)^2\pi^{-2}R_0^{-2} - \pi^{-2}g(\zeta)^2) \\ &= L_z^2(c^{-2}\pi^{-2}\omega^2 - (\chi_m^n)^2\pi^{-2}R_0^{-2}) - L_z^2(\pi^{-2}g(\zeta)^2 - (\chi_m^n)^2\pi^{-2}R_0^{-2}) \end{aligned} \quad (4.18)$$

then from eq.4.18, a parameter  $a$  and  $2q \cos(2\zeta)$  of the Mathieu equation is

$$\begin{aligned} a &= L_z^2(c^{-2}\pi^{-2}\omega^2 - (\chi_m^n)^2\pi^{-2}R_0^{-2}) \\ &= \hat{\omega}^2 - \hat{\omega}_c^2 \end{aligned} \quad (4.19)$$

here we define a dimensionless parameter; a normalized angular frequency  $\hat{\omega}$

$$\hat{\omega} = \frac{L_z}{\pi c} \omega \quad (4.20)$$

and a normalized cut-off angular frequency  $\hat{\omega}_c$

$$\hat{\omega}_c = \frac{\chi_m^n L_z}{\pi R_0} \quad (4.21)$$

The cosine term of Mathieu function can be expressed as

$$\begin{aligned} 2q \cos(2\zeta) &= L_z^2 (\pi^{-2} g(\zeta)^2 - (\chi_m^n)^2 \pi^{-2} R_0^{-2}) \\ g(\zeta) &= \pi \left( (\chi_m^n)^2 \pi^{-2} R_0^{-2} + 2L_z^{-2} q \cos(2\zeta) \right)^{\frac{1}{2}} \end{aligned} \quad (4.22)$$

A boundary condition at  $R(z)$  ( $R(z)$  is the radius of the cylindrical corrugated waveguide which a function depends on  $z$ ), electric field which is tangent to the corrugated side ( $\mathbf{E}_{\parallel}$ ) is equal to the error at the boundary  $\varepsilon_{Bdd}$

$$\begin{aligned} \varepsilon_{Bdd} &= \tilde{\mathbf{E}} \cdot \frac{1}{(1 + R'^2)^{\frac{1}{2}}} (\mathbf{e}_z + R' \mathbf{e}_r) \\ &= -B_0 (1 + R'^2)^{\frac{1}{2}} g^{-1} [R' (g\eta\phi' - g'\eta) J_1 + (RR'g' - g)g\phi J_0] \end{aligned} \quad (4.23)$$

When  $R'(z)$  is 0 in the smooth corrugated, the error at the boundary is 0 (similar to a uniform cylindrical waveguide where  $\tilde{\mathbf{E}}_{\parallel}|_{Bdd} = 0$ ), then  $E_{\parallel}$  is

$$\varepsilon_{Bdd} = 0 = B_0 g(\zeta) \phi(\eta z) J_0(R(z)g(\zeta)) \quad (4.24)$$

the Bessel functions of the first kind,  $J_0(R(z)g(\zeta)) = 0$  when

$$R(z)g(\zeta) = \chi_m^n \quad (4.25)$$

because we consider the  $\text{TM}_{01}$  mode, so  $\chi_0^1$  is the solution. Then, the radius function of the cylindrical corrugated waveguide is

$$\begin{aligned} R(z) &= \frac{\chi_0^1}{g(\zeta)} \\ &= \chi_0^1 \pi^{-1} \left( (\chi_0^1)^2 \pi^{-2} R_0^{-2} + 2L_z^{-2} q \cos(2\zeta) \right)^{-\frac{1}{2}} \\ &= \left( R_0^{-2} + 2(\chi_0^1)^{-2} \pi^2 L_z^{-2} q \cos(2\zeta) \right)^{-\frac{1}{2}} \end{aligned} \quad (4.26)$$

The  $R(z)$  is a function we use to define the structure of a corrugated waveguide structure. By applying Taylor's expansion to eq.4.26,  $q$  is assumed to be small

$$R(z) \approx R_0 \left( 1 - (\chi_0^1)^{-2} \pi^2 R_0^2 L_z^{-2} q \cos(2\zeta) \right) \quad (4.27)$$

from this expansion, we can see that the radius of the cylindrical  $R(z)$  will oscillate around the value of  $R_0$ .

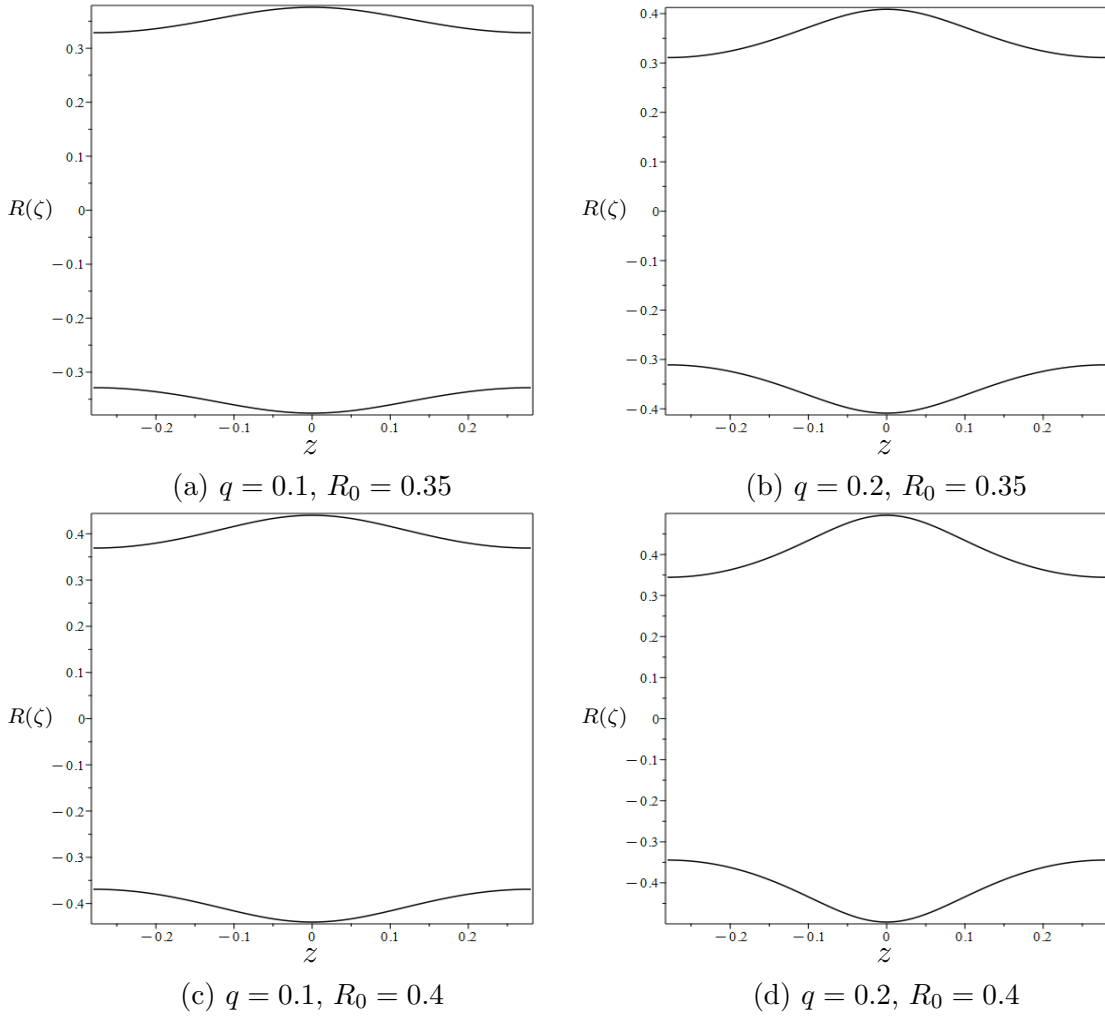


Figure 4.1: The cylindrical corrugated profile when varying parameter  $q$  and  $R_0$ .

## 4.5 The Ansatz Optimization

Recalling the error of an approximation in the Faraday's Law

$$\begin{aligned} \varepsilon_{Max} = & (0)\mathbf{e}_r - B_0\left\{[-g''g^{-1}\phi + (-g'^2r^2 + 2g'^2g^{-2})\phi - \frac{g'g^{-2}\eta\phi}{2}]J_1 \right. \\ & \left. + \left[\frac{g'\eta\phi}{2} + g''\eta - g'^2g^{-2}\phi\right]rJ_0\right\}\mathbf{e}_\theta + (0)\mathbf{e}_z \end{aligned} \quad (4.28)$$

and the error at the boundary  $\tilde{\mathbf{E}}_{\parallel}|_{Bdd} = \varepsilon_{Bdd}$

$$\varepsilon_{Bdd} = -B_0(1 + R'^2)^{\frac{1}{2}}g^{-1}[R'(g\eta\phi' - g'\eta)J_1 + (rR'g' - g)g\phi J_0]|_{r=R(z)} \quad (4.29)$$

We can notice that both errors depend on factors  $g'$ ,  $g''$  or  $R'$ . From eq.4.26  $g'$  and  $g''$  in term of  $R(\eta z)$  are

$$g'(\eta z) = -\chi_0^1\eta R(\eta z)^{-2}R'(\eta z) \quad (4.30)$$

$$g''(\eta z) = 2\chi_0^1\eta^2 R(\eta z)^{-3}R'(\eta z)^2 - \chi_0^1\eta^2 R(\eta z)^{-2}R''(\eta z) \quad (4.31)$$

The smaller of  $R'$  and  $R''$  are, the smaller of the errors of an approximation. When the  $R'$  and  $R''$  are small, the corrugated wall is smooth. This means if we want a good approximation, we have to keep the corrugation smooth.

From eq.4.22 and 4.26,  $g'$  and  $g''$  are

$$g'(\pi L_z^{-1}z) = -\frac{2\pi^3 q}{L_z^3 g(\pi L_z^{-1}z)} \sin(2\pi L_z^{-1}z) \quad (4.32)$$

and

$$g''(\eta z) = -\frac{4\pi^6 q^2}{L_z^6 g(\pi L_z^{-1}z)^3} \sin^2(2\pi L_z^{-1}z) - \frac{4\pi^4 q}{L_z^4 g(\pi L_z^{-1}z)} \cos(2\pi L_z^{-1}z) \quad (4.33)$$

with the fixed  $q$  and  $R_0$ , the errors  $\varepsilon_{Max}$  and  $\varepsilon_{Bdd}$  approach zero when  $L_z^{-3} \rightarrow \infty$ .

We can define this condition when the errors go to zero as a dimensionless factor  $\delta$ .

$$\delta = \frac{R_0}{L_z} \quad (4.34)$$

With the parameter  $\delta$ , we could predict that our approximation would be getting better when the value of  $\delta$  is getting smaller (approach 0).

## 4.6 Summary of a chapter 4

Chapter 4 is the continue work from the rectangular corrugated waveguide [16], so the mathematical process for finding solutions of Maxwell's equations is similar to chapter 3 section 1, but with more details. We start with modified Maxwell's equations (4.1-4.4) and boundary conditions eq.4.5. By substituting the magnetic field equation of the cylindrical corrugated waveguide eq.4.7 into Maxwell's eq.4.4, we obtain the electric field eq.4.8.

In section 4.2, we show that from our modified Maxwell's equations (Faraday's law eq.4.3), we can manipulate the error ( $\epsilon_{Max}$ ) to be small for the good approximation. From minimizing the  $\epsilon_{Max}$ , we get the function of  $\phi(\zeta)$  which will be rewritten into Mathieu equation in section 4.4. In addition, we found 2 constrains to be considered when designing the cylindrical corrugated waveguide. Firstly, at the center of waveguide, we get the best approximation due to  $\epsilon_{Max} = 0$ . Secondly, The smaller the parameter  $q$  is, the better the approximation.

We consider the electromagnetic field at the boundary in section 4.3, we get the equation of the tangent electric field at the boundary  $\tilde{\mathbf{E}}_{\parallel}$  eq.4.15 which will be considered further in section 4.4.

By rewriting  $\phi(\zeta)$  eq.4.10 into Mathieu eq.4.16 in section 4.4, we found a normalized angular frequency  $\hat{\omega} = (L_z\omega)/(\pi c)$  and a  $\text{TM}_{01}$  normalized cut-off angular frequency  $\hat{\omega}_c = (\chi_0^1 L_z)/(\pi R_0)$ , where  $\chi_0^1$  is the 1<sup>st</sup> root of  $J_0$ , and  $R_0$  is an average radius of the structure. Furthermore, we define our model to have a smooth corrugated,  $\tilde{\mathbf{E}}_{\parallel}|_{Bdd} = \epsilon_{Bdd} = 0$ . Therefore, the radius function of the cylindrical corrugated waveguide is  $R(z) \approx R_0 \left( 1 - (\chi_0^1)^{-2} \pi^2 R_0^2 L_z^{-2} q \cos(2\zeta) \right)$ .

In addition, section 4.5 is an optimization of the ansatz. We find that by adjusting  $\delta = R_0/L_z$  to be small (approach 0), we expect to receive a good approximation of our analytical results.

# Chapter 5

## CST Simulation of the Cylindrical Corrugated Waveguide

CST or Computer Simulation Technology is a software package for analyzing 3-dimension of the electromagnetic field. We use CST to find the numerical solutions of the electromagnetic field inside the cylindrical corrugated waveguide and compare these results with the analytical results. We begin with creating the corrugated cylindrical structure with geometry  $q = 0.1$ ,  $R_0 = 0.36$  mm,  $L_z = 0.59$  mm, and  $\hat{\omega}_c \approx 1.254$ .

However, we need to be reminded that the accuracy of the numerical results depends on many factors, such as solver options, mesh types, the density of the mesh. So, there are still more areas for an improvement in the numerical accuracy, and this will be our future works.

### 5.1 Set Up the Conditions for Simulation

Before running a simulation, we set up the conditions in the following steps.

1. In Home → Click a drop-down of Setup Solver → Select Eigenmode Solver.



2. Because the structure is vacuum, we set a background properties to be a Perfect Electric Conductor (PEC).

In Simulation → Click Background → Choose Material type: PEC.

## 5.1. SET UP THE CONDITIONS FOR SIMULATION

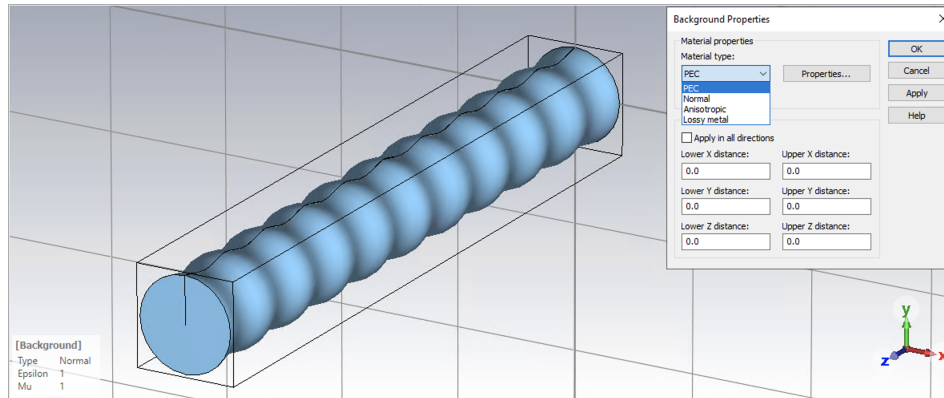


Figure 5.1: For a Background Properties setup, chose Material type to be PEC.

3. For the boundary conditions, we set the tangential electric field ( $E_t = 0$ ) at boundaries (at the corrugated wall, the beginning, and the end of the waveguide) equal to 0. So, this structure is basically the resonant cavity, forming the standing electromagnetic waves. Alternatively, we can choose  $E_t = \text{periodic}$  which has the property of  $E(z) = E(z + L_z)$ . However, the amplitude of the electric field always starts at  $z = 0$  in the first condition, making it easy to compare the numerical results to the analytical results.

In Simulation → Click Boundaries → Choose “electric ( $E_t = 0$ )” in all directions.

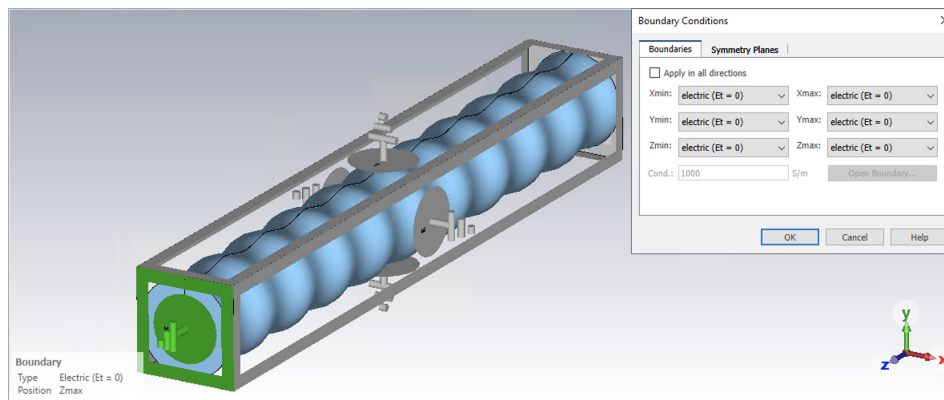


Figure 5.2: For a Boundary Conditions setup, choose “electric ( $E_t = 0$ )” in all directions.

4. We can refine mesh of a structure with Global Properties

## 5.1. SET UP THE CONDITIONS FOR SIMULATION

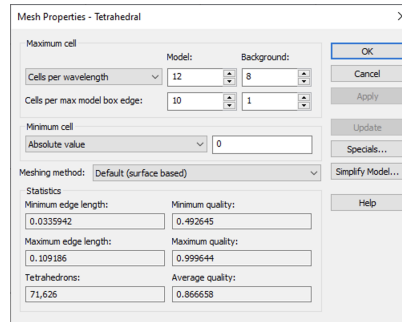


Figure 5.3: For a Boundary Conditions setup, choose “electric ( $Et = 0$ )” in all directions.

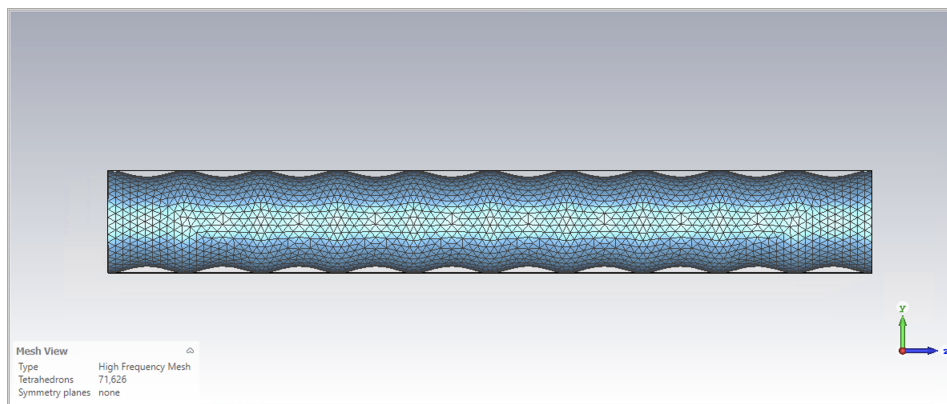


Figure 5.4: For a Boundary Conditions setup, choose “electric ( $Et = 0$ )” in all directions.

5. In Simulation → Click Setup Solver → Set up Eigenmode Solver Parameters.

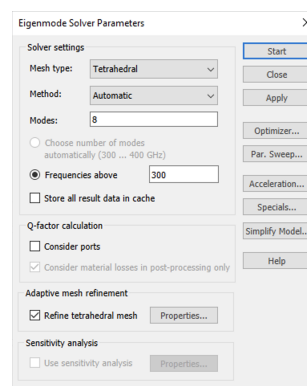


Figure 5.5: For Eigenmode Solver Parameters.

## 5.1. SET UP THE CONDITIONS FOR SIMULATION

Fig.5.6 shows one of the simulation results of the corrugated cylindrical structure with geometry  $q = 0$ ,  $R_0 = 0.36$  mm,  $L_z = 0.59$  mm, a periods of the corrugation  $n = 10$  and  $\hat{\omega}_c \approx 1.254$ . The electric field  $TM_{01}$  in a cross-section  $y - z$  plane has frequency 327.028 GHz and we can calculate a normalized wavenumber by a wavenumber and geometry of the structure.

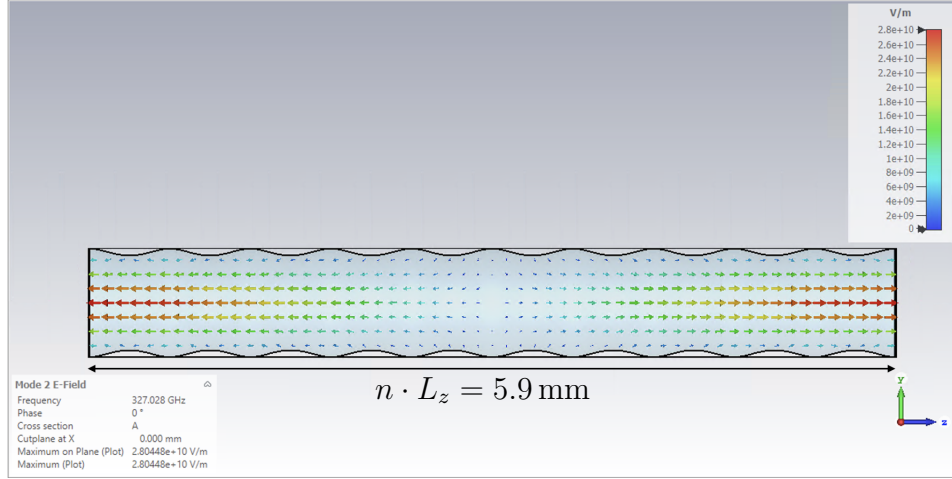


Figure 5.6: The example of the  $TM_{01}$  mode electric field simulated by CST.

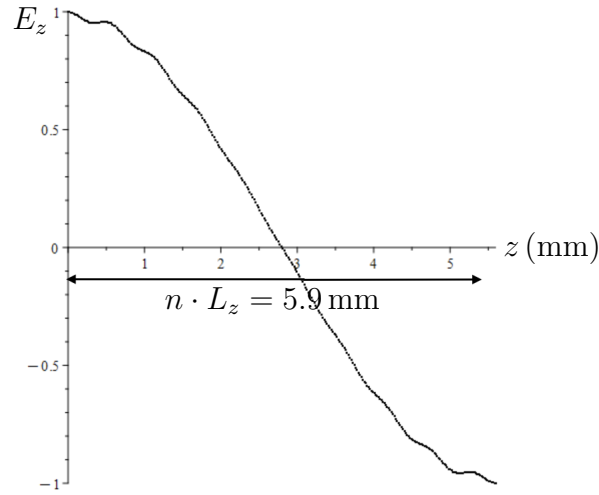


Figure 5.7: The graph of a normalized longitudinal electric field and  $z$ , plotting from data of a simulation fig.5.6.

The relation between normalized wavenumbers  $\hat{k}$  and wavenumbers  $k$

$$\begin{aligned} \hat{k} &= \frac{L_z}{\pi} k \\ &= \frac{L_z}{\pi} \frac{2\pi}{\lambda} \end{aligned} \quad (5.1)$$

from fig5.7, wavelength of the electric field is

$$\begin{aligned}\nu\lambda &= n \cdot L_z \\ \lambda &= \frac{n \cdot L_z}{\nu}\end{aligned}\tag{5.2}$$

where  $\nu$  is the number of waves, substitute  $\lambda$  in eq.5.2 to eq.5.1

$$\begin{aligned}\hat{k} &= \frac{L_z}{\pi} k \\ &= \frac{2\pi L_z}{\pi} \frac{\nu}{n \cdot L_z} \\ &= \frac{2\nu}{n}\end{aligned}\tag{5.3}$$

For example, the longitudinal electric field  $E_z$  in fig.5.6 or fig.5.7 has  $n = 10$ , and the number of wave is  $1/2$ , therefore  $\hat{k}$  is

$$\hat{k} = \frac{2\nu}{n} = \frac{2 \cdot 1}{10 \cdot 2} = 0.1\tag{5.4}$$

## 5.2 Analytical and Numerical Results Comparison

The analytical result of Maxwell's equations for the TM01 electric field at the center  $r = 0$

$$\mathbf{E}_z = B_0 g(\eta z) \phi(\eta z) J_0(0) \mathbf{e}_z\tag{5.5}$$

we use Maple software to generate graphs of the normalized longitudinal electric field  $E_{zn}$  and  $z$  from eq.5.5 then compare these results to the data from CST simulation. We analyze the corrugated cylindrical structure with geometry  $q = 0$ ,  $R_0 = 0.36$  mm,  $L_z = 0.59$  mm, periods of corrugation  $n = 10$  and  $\hat{\omega}_c \approx 1.254$ . These comparisons are shown in fig.5.8.

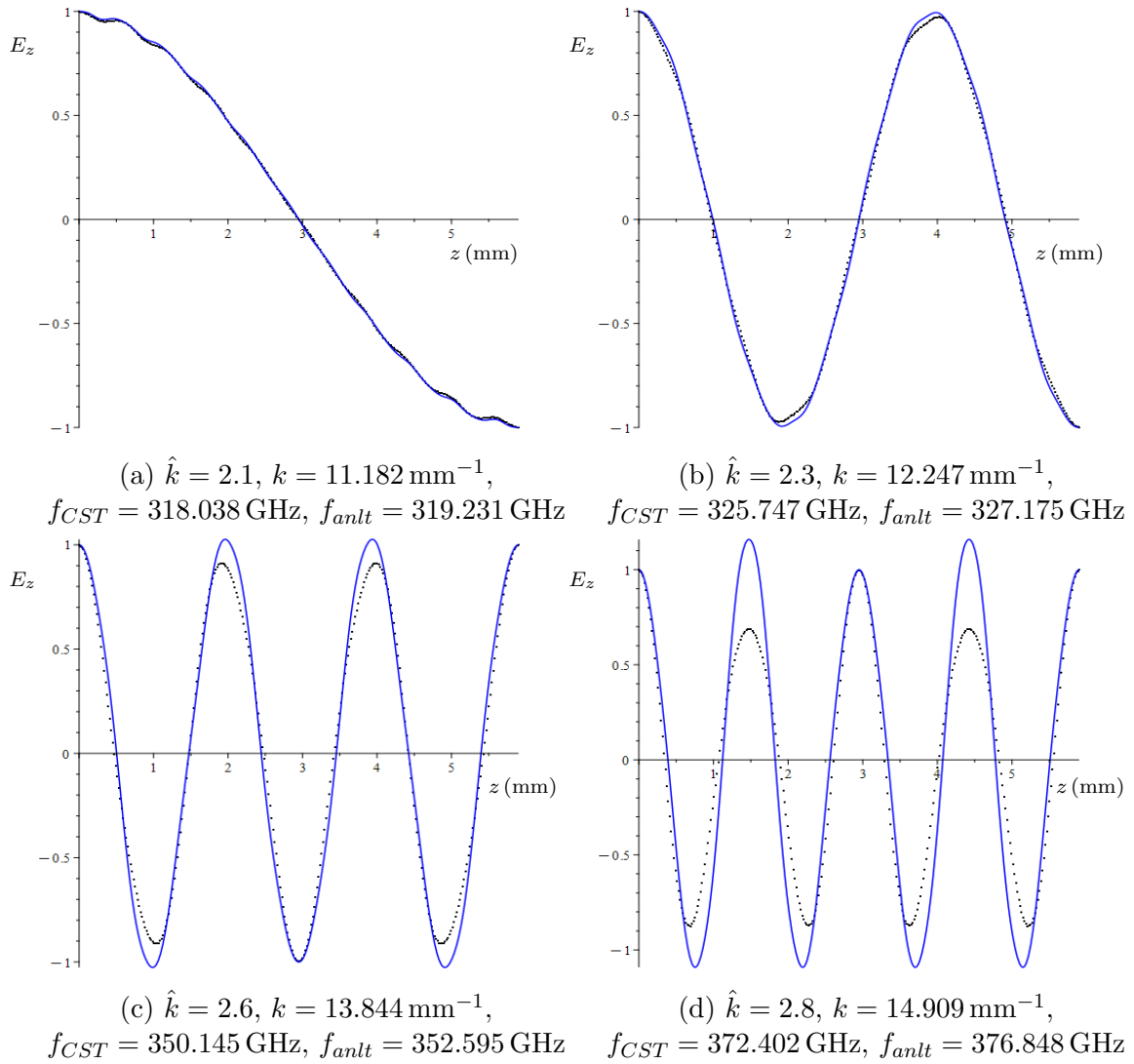


Figure 5.8: The normalized longitudinal electric fields  $\text{TM}_{01}$ ,  $E_z$  at the center  $x = 0$ ,  $y = 0$ , or  $r = 0$  of the cylindrical corrugated waveguide with geometry  $q = 0.1$ ,  $R_0 = 0.36 \text{ mm}$ , and  $L_z = 0.59 \text{ mm}$ , periods of corrugation  $n = 10$  and  $\hat{\omega}_c \approx 1.254$ . The blue graph is an analytical result and the black dot line is the numerical result from CST simulation.

The results show better matching in the graph than the rectangular corrugated waveguide. When  $k$  is small, the graph of these two results are nearly align perfectly. However, when  $\hat{k}$  increases, there are differences in the peak between these graphs. we also collect the data both analytical and numerical results as shown in table 5.1 to plot the dispersion relation. We found the CIP of the analytical dispersion is  $\hat{k}_{CIP} = 2.857$ ,  $k_{CIP} = 15.213 \text{ mm}^{-1}$ ,  $\hat{\omega}_{CIP} = 1.513$ ,  $f_{CIP} = 384.464 \text{ GHz}$ , and  $\beta_e = 0.53$ .

$\hat{k}$	$k$	Analytic		Numeric	
		$f$ (GHz)	$\hat{\omega}$	$f$ (GHz)	$\hat{\omega}$
2.1	11181.94	319.231	1.257	318.038	1.252
2.2	11714.413	322.234	1.268	320.955	1.263
2.3	12246.887	327.175	1.288	325.747	1.282
2.4	12779.36	333.965	1.315	332.311	1.308
2.5	13311.833	342.485	1.348	340.508	1.340
2.6	13844.307	352.595	1.388	350.145	1.378
2.7	14376.78	364.126	1.433	360.947	1.421
2.8	14909.253	376.848	1.483	372.402	1.466
2.9	15441.727	390.21	1.536	383.134	1.508
3.0	15974.2	399.501	1.572	388.515	1.529

Table 5.1: Collection of data from the analytical and numerical result of the cylindrical corrugated waveguide  $q = 0.1$ ,  $\omega_c \approx 1.254$ .

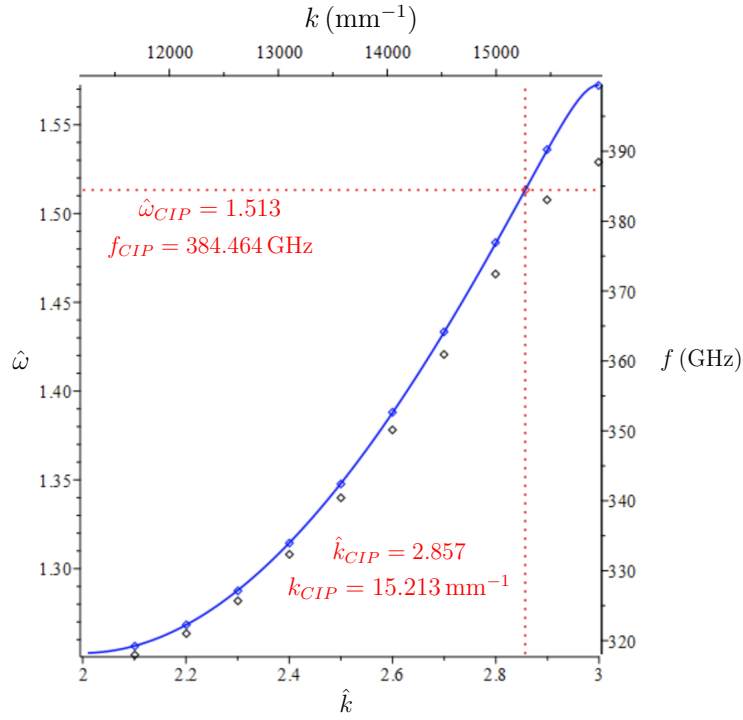
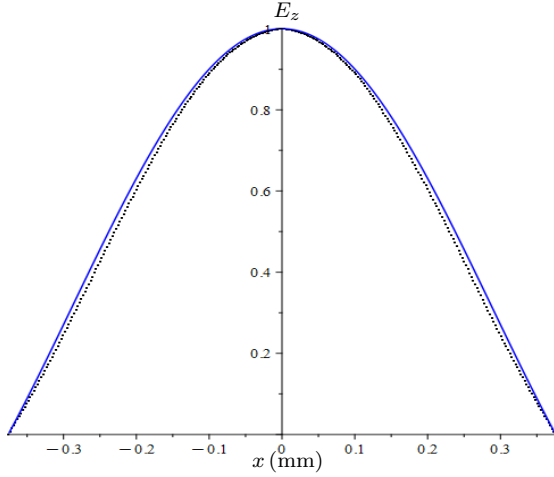
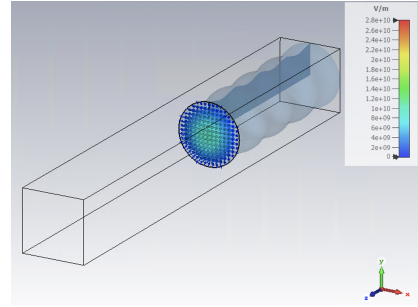


Figure 5.9: The dispersion relation result from CST (black dots) and analytical equation (blue line and blue dots) of the cylindrical corrugated waveguide with geometry  $q = 0.1$ ,  $R_0 = 0.36 \text{ mm}$ , and  $L_z = 0.59 \text{ mm}$ , periods of corrugation  $n = 10$  and  $\omega_c \approx 1.254$ . The CIP for analytical results of this structure is  $\hat{k}_{CIP} = 2.857$ ,  $k_{CIP} = 15.213 \text{ mm}^{-1}$ ,  $\hat{\omega}_{CIP} = 1.513$ ,  $f_{CIP} = 384.464 \text{ GHz}$ , and  $\beta_e = 0.53$ .

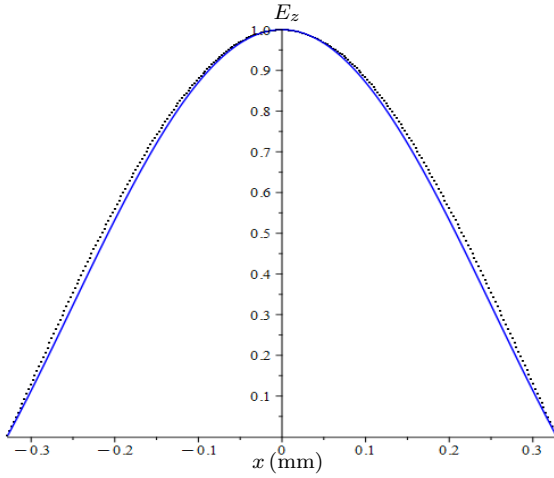
In addition, we examine if our analytical models can be used with another point beside  $r = 0$ . In fig.5.10 we observe the longitudinal electric field  $E_z$  in the  $x - y$  cross-section at the widest  $z = 4L_z$  and the narrowest  $z = 6.5L_z$  of the cylindrical corrugated waveguide with geometry  $q = 0.1$ ,  $R_0 = 0.35$  mm, and  $L_z = 0.56$  mm, periods of corrugation  $n = 10$  and  $\hat{\omega}_c \approx 1.225$ . We can observe the good matching of these two graphs of  $E_z$  in the  $x - y$  cross-section.



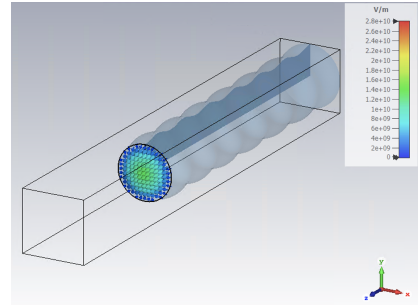
(a)  $\hat{k} = 2.1$ ,  $x - y$  cross-section at  $z = 4L_z$



(b) Cross-section  $x - y$  axis of model by CST at  $z = 4L_z$



(c)  $\hat{k} = 2.1$ ,  $x - y$  cross-section at  $z = 6.5L_z$



(d) Cross-section  $x - y$  axis of model by CST at  $z = 6.5L_z$

Figure 5.10: A graph of the normalized longitudinal electric field  $TM_{01}$  mode of the cylindrical corrugated waveguide and distance in  $z$ -direction at cross-section  $x - y$ . The  $TM_{01}$  mode of the normalized longitudinal electric fields  $E_z$  at  $z = 4L_z$  of the cylindrical corrugated waveguide with geometry  $q = 0.1$ ,  $R_0 = 0.35$  mm, and  $L_z = 0.56$  mm, periods of corrugation  $n = 10$  and  $\hat{\omega}_c \approx 1.225$ . The blue graph is an analytical electric field and the black dot line is the numerical result from CST simulation.

### 5.3 Phase and Group Velocities

We observe the CIP of analytical and numerical results by generating graphs of phase and group velocities and observe the point where there is the coincide of these two plots.

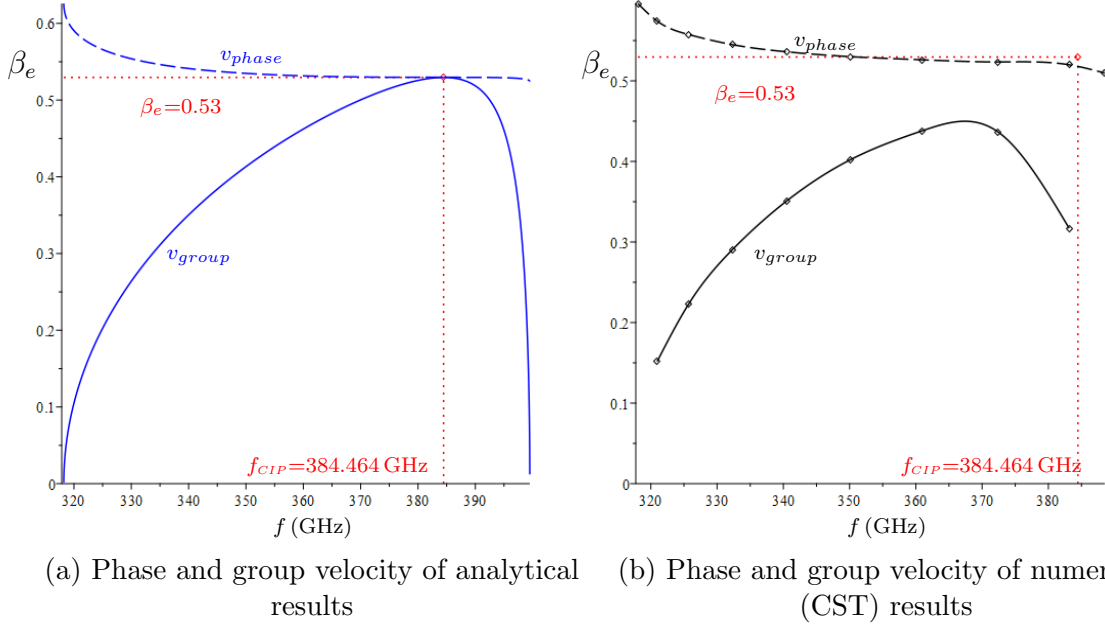


Figure 5.11: Phase velocities (dash line) and group velocities (solid line) of analytical results (blue) and numerical results (black) of the cylindrical corrugated waveguide  $q = 0.1$ ,  $R_0 = 0.36$  mm,  $L_z = 0.59$  mm,  $n = 10$ , and  $\hat{\omega}_c \approx 1.254$ . The CIP of analytical results is  $f_{CIP} = 384.464$  GHz, and  $\beta_e = 0.53$  (92 KeV).

Fig.5.11 shows graphs of analytical phase and group velocities (5.11a) and numerical phase and group velocities (5.11b) of the structure  $q = 0.1$ ,  $R_0 = 0.36$  mm,  $L_z = 0.59$  mm,  $n = 10$ , and  $\hat{\omega}_c \approx 1.254$ . For analytical results, there is the CIP at  $f_{CIP} = 384.464$  GHz and  $\beta_e = 0.53$  (92 KeV) exactly the same point which predicted by the mathematic model. However, we cannot find the CIP of the numerical results from this geometry. Therefore, we change the geometry of the structure, result to  $\hat{\omega}_c$  be varied. Then, plot the results of phase and group velocities from this varying to find the CIP of numerical results as shown in fig.5.12.

### 5.3. PHASE AND GROUP VELOCITIES

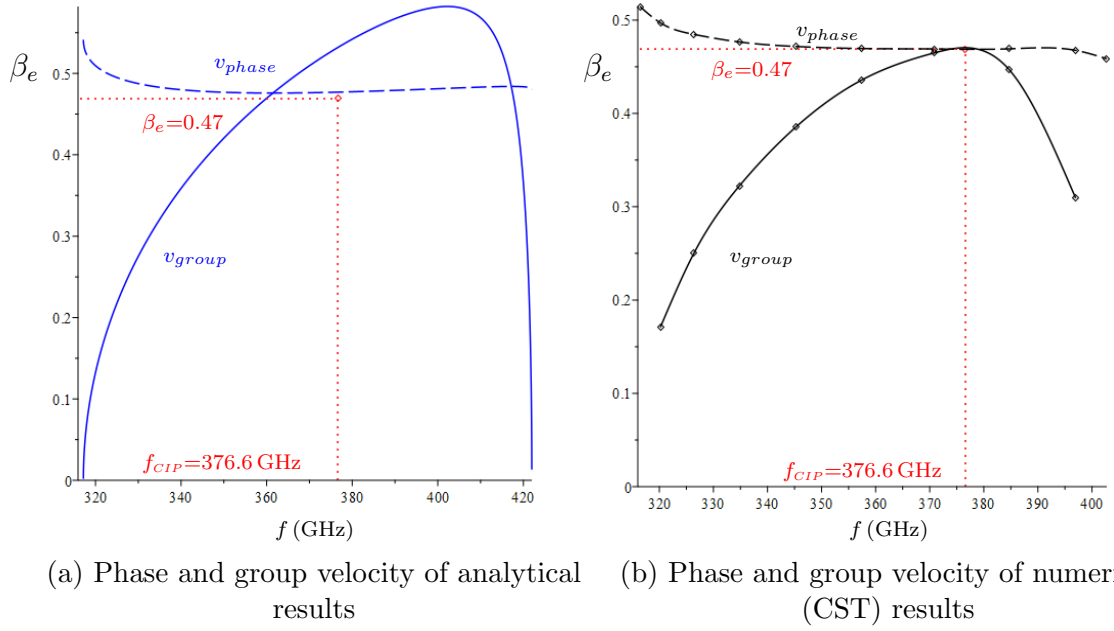


Figure 5.12: Phase velocities (dash line) and group velocities (solid line) of analytical results (blue) and numerical results (black) of the cylindrical corrugated waveguide  $q = 0.1$ ,  $R_0 = 0.361$  mm,  $L_z = 0.512$  mm,  $n = 10$ , and  $\hat{\omega}_c \approx 1.086$ . The CIP of numerical results is  $f_{CIP} = 376.6$  GHz, and  $\beta_e = 0.47$  (68 KeV).

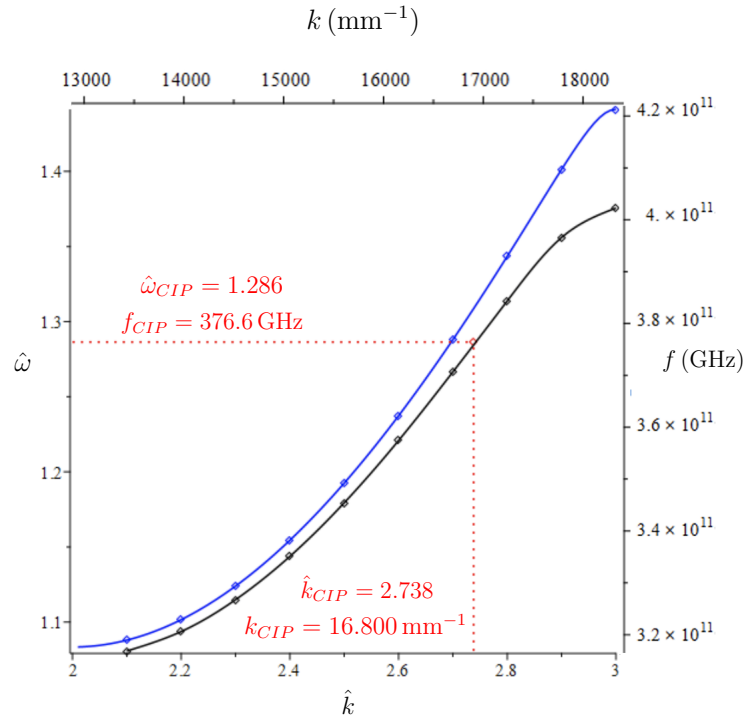


Figure 5.13: The dispersion relation results from CST (black dots) and analytical results (blue line and blue dots) of the cylindrical corrugated waveguide with geometry  $q = 0.1$ ,  $R_0 = 0.361$  mm,  $L_z = 0.512$  mm,  $n = 10$ , and  $\hat{\omega}_c \approx 1.086$ . The CIP for analytical results of this structure is  $\hat{k}_{CIP} = 2.738$ ,  $k_{CIP} = 16.800$   $\text{mm}^{-1}$ ,  $\hat{\omega}_{CIP} = 1.286$ ,  $f_{CIP} = 376.6$  GHz, and  $\beta_e = 0.47$  (68 KeV).

From fig. 5.12, we found that for the cylindrical corrugated waveguide  $q = 0.1$ ,  $R_0 = 0.361$  mm,  $L_z = 0.512$  mm,  $n = 10$ , and  $\hat{\omega}_c \approx 1.086$ , there is no the CIP of the analytical results fig.5.12a. In the other hand, for numerical results, there is the CIP at  $f_{CIP} = 376.6$  GHz and  $\beta_e = 0.47$  (68 KeV).

The dispersion relation of the cylindrical corrugated waveguide  $q = 0.1$ ,  $R_0 = 0.361$  mm,  $L_z = 0.512$  mm,  $n = 10$ , and  $\hat{\omega}_c \approx 1.086$  is shown in fig.5.13. There are noticeable differences in results between analytical results and numerical results for this value of  $\hat{\omega}_c \approx 1.086$ , comparing to  $\hat{\omega}_c \approx 1.254$  in fig.5.9 which has a better agreement.

## 5.4 Variation of $\delta$ and $q$

From our models, we predict that for a small value of  $\delta = R_0/L_z$  and  $q$ , we will get the good approximation. Therefore, we examine the graphs between analytical and numerical results when  $\delta$  and  $q$  is varied.

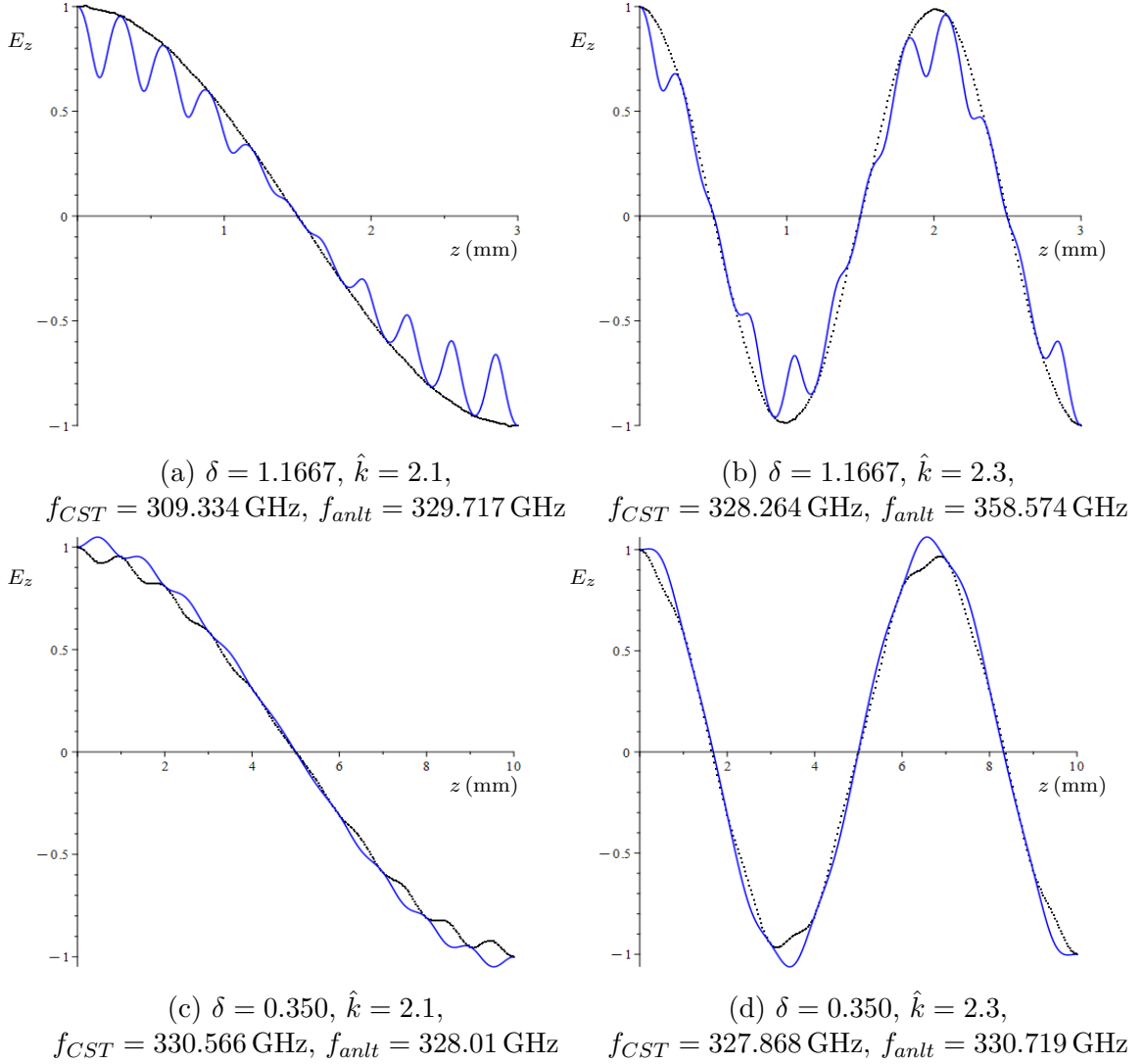


Figure 5.14: The  $TM_{01}$  mode of the normalized longitudinal electric fields  $E_z$  at the center  $x = 0, y = 0$ , or  $r = 0$  of the cylindrical corrugated waveguide with geometry  $q = 0.1, R_0 = 0.35 \text{ mm}$ , periods of corrugation  $n = 10$ . For (a) and (b)  $L_z = 0.3 \text{ mm}$  and  $\delta = 1.1667$ , and  $\hat{\omega}_c = 0.656$ . For (c) and (d)  $L_z = 1.0 \text{ mm}$ ,  $\delta = 0.350$ , and  $\hat{\omega}_c = 2.187$ . The blue graph is analytical results and the black dot line is numerical results from CST simulation.

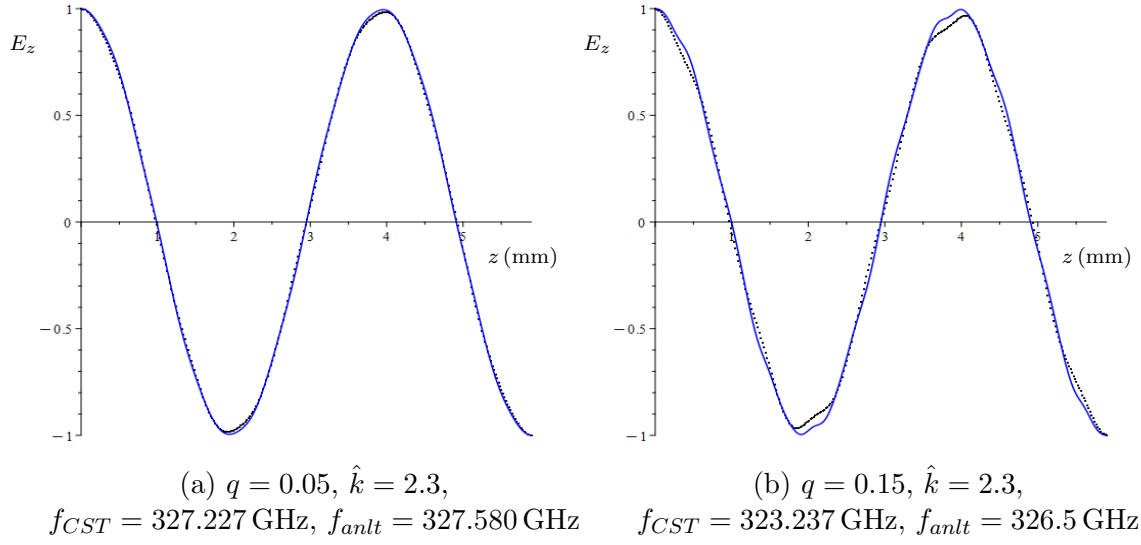


Figure 5.15: The  $TM_{01}$  mode of the normalized longitudinal electric fields  $E_z$  at the center  $x = 0, y = 0$ , or  $r = 0$  of the cylindrical corrugated waveguide with geometry  $R_0 = 0.36$  mm, periods of corrugation  $n = 10$  with different  $q$ . For (a) and (b)  $q = 0.05$ , (c) and (d)  $q = 0.15$ . The blue graph is analytical results and the black dot line is numerical results from CST simulation.

From fig.5.15, the results follow our prediction, when  $q$  is small, we receive a better agreement in analytical and numerical results. However, this prediction does not apply to the value of  $\delta$ . Instead of getting the good matching when  $\delta = 0.350$ , we can observe the unmatched graphs. The best results we get are when the  $\delta$  is equal to 0.610, which is the cylindrical corrugated waveguide with  $R_0 = 0.36$  mm and  $L_z = 0.59$  mm in fig.5.8.

## 5.5 Summary of a chapter 5

In section 5.1, we demonstrate the set up for CST studio step by step. The geometry of our structure is  $q = 0.1$ ,  $R_0 = 0.36$  mm,  $L_z = 0.59$  mm, and  $\hat{\omega}_c \approx 1.254$ . The CIP of this structure is  $\hat{k}_{CIP} = 2.857$ ,  $\hat{\omega}_{CIP} = 1.513$ ,  $f_{CIP} = 384.464$  GHz, and  $\beta_e = 0.53$  (92 KeV). We use eigenmode solver to find the results of Maxwell's equations. The boundary condition is a perfect electric conductor, PEC. Therefore this condition allows the amplitude of an electric field always starts at  $z = 0$ , this makes it easy to compare numerical results to analytical results. Then we can export the data of the longitudinal electric fields  $TM_{01}$  ( $E_z$ ) at any positions ( $z$ ). We identify  $\hat{k}$  of the mode from CST by using eq.5.3.

By exploiting CST studio, we compare analytical results and numerical results in section 5.2, and can observe a good agreement between these two results fig.5.8. In addition, we examine the off-center electric field of the waveguide  $q = 0.1$ ,  $R_0 = 0.35$  mm, and  $L_z = 0.56$  mm, periods of corrugation  $n = 10$  and  $\hat{\omega}_c \approx 1.225$ . As a result, we also found a good match between analytical results and numerical results as well (fig.5.10).

However, the CIP for numerical results is not the same as the results from analytic. From phase and group velocities graph in section 5.3, we found the CIP from the point where phase velocities, group velocities, and the velocity of particle ( $\beta_e$ ) of results from CST are coincided. Hence, for the cylindrical corrugated waveguide  $q = 0.1$ , the CIP of numerical results is available for the structure  $R_0 = 0.361$  mm,  $L_z = 0.512$  mm, and  $\hat{\omega}_c \approx 1.086$ . The CIP for this structure is  $\hat{k}_{CIP} = 2.738$ ,  $\hat{\omega}_{CIP} = 1.286$ ,  $f_{CIP} = 376.6$  GHz, and  $\beta_e = 0.47$ (68 KeV) as shown in fig.5.12.

Regarding section 4.2 and 4.5, we expect to observe a better agreement of analytical and numerical results when  $\delta = R_0/L_z$  and  $q$  are very small (approach 0). From a fig.5.14, when  $\delta$  is small ( $\delta = 0.350$ ), instead of the good matching plot from these two results, we found the unmatched which does not follow our prediction. In the other hand, our prediction can apply when  $q$  is small as shown in fig.5.15. The graph between analytical and numerical results has a better correspondence when  $q = 0.05$ , comparing to a graph which  $q = 0.15$ .

# Chapter 6

## Future Works

In this section we will discuss the future direction of the theoretical work that can advance the goal of making the cylindrical corrugated waveguide.

### The Delta and an Approximation

From our approximation, we predict that the smaller the  $\delta$  is ( $\delta = \frac{R_0}{L_z}$  for the cylindrical corrugated waveguide and  $\delta = \frac{L_0}{L_z}$  for the rectangular corrugated waveguide), the better of an approximation it will be. We first observe the cylindrical corrugated waveguide with  $\delta = 0.6102$  in fig.5.8, the analytical results give a good matching graph with the results from CST. However, when the  $\delta$  increases to  $\delta = 1.1667$  and decreases to  $\delta = 0.350$  in fig.5.14, the analytical results are not close to the numerical results. This lead to the future works to improve our approximation, we found that by dividing the magnetic field in eq.4.7 by  $g(\eta z)$  can improve the analytical results to get a good matching with numerical results when  $\delta$  is small (less than  $\delta = 0.6102$ )

$$\tilde{\mathbf{B}} = B_0 c^{-2} (-i\omega) g(\eta z)^{-1} \phi(\eta z) J_1(r g(\eta z)) \mathbf{e}_\theta \quad (6.1)$$

then the longitudinal electric field  $\text{TM}_{01}$  mode at the center of the waveguide will be

$$\tilde{\mathbf{E}} = B_0 \phi(\eta z) J_0(r g) \mathbf{e}_z \quad (6.2)$$

Furthermore, we also can improve analytical solutions for the rectangular corrugated waveguide with the division by  $(\kappa_x^2 + \kappa_y^2)$  in the magnetic field eq.3.3. Therefore, the longitudinal electric field  $\text{TM}_{11}$  mode at the center of the waveguide will be

$$\tilde{\mathbf{E}} = B_0 \cos(\kappa_x x) \cos(\kappa_y y) \phi(\eta z) \mathbf{e}_z. \quad (6.3)$$

and we will find the reasons why the first model does not work like the prediction.

### CIP of Numerical Results from CST

As shown in fig.5.11 and fig.5.12, the CIP of analytical results and numerical results are not the same. We find the numerical CIP by running the simulation CST with the variant of geometry parameters. In this thesis, we set up the periods of corrugations equal to 10, this makes the scale of  $\hat{k}$  is 0.1, then we utilize the interpolate function in Maple software and draw a phase and group velocity graph. We can improve

---

these results by applying periods of corrugation to be more than 10. For example, in fig.3.7 the work by [16] the periods of corrugation is 20, so the of  $\hat{k}$  will be finer to 0.05. Furthermore, we will find the right factors (the set up of the simulation) that will improve the accuracy of numerical results.

## Simulation with Particles

We will use our model, the cylindrical corrugated waveguide to examine the particles-electric field interaction by Particle-in-Cell simulator or PIC in CST particle studio. We have the structure with  $q = 0$ ,  $R_0 = 0.36\text{mm}$ ,  $L_z = 0.59\text{mm}$ , and  $\hat{\omega}_c \approx 1.255$ , we know the CIP from analytical results  $\hat{k} = 2.857$ ,  $f = 384.464$  GHz that would interact with the particles with velocity  $0.53c$ . Firstly, we will observe an input continue DC beam imported to the structure, we expect to see the output signal if there is an interaction occurred. Another way to test the particle-beam interaction, injecting a bunch of Gaussian beam, this is more practical compare to the DC beam. If an interaction occurred, we could detect the rising in amplitude of the signal.

## Experimental Prototype

After we have examined the interaction between particles and an electric field, the next step is producing the experimental prototype. By using the optic fiber extrusion technique, we would fabricate the sub-millimeter cylindrical corrugated waveguide regarding the geometry in eq.4.26. However, this is a challenge for us to working on in the future. Because there have not been the works on this type of structure yet, in common the optical fibers are manufactured in the cylinder shape to send the signal via light. We expect that with varying the speed of extrusion, the cylindrical corrugation shape would be constructed.

# Chapter 7

## Conclusion

We show that for our symmetric corrugated waveguide, both the rectangular and the cylindrical corrugated waveguide can accelerate particles and allow particle to exchange the energy with the electromagnetic field to generate terahertz radiation. With the fiber optic extrusion technique, we can manufacture the cylindrical corrugated structure in the scale of sub-millimeter and the cost is relatively lower than making the rectangular corrugated waveguide by CNC.

By modifying the magnetic field with  $\phi(\eta z)$  which can be solved by Mathieu equation, we can find the relation explicit approximate solutions of magnetic fields and electric fields. We aim to find the geometry of the structure corresponds to the defining point on the dispersion relation, the coincident inflection point (CIP) where particles would interact with broad frequencies range electric field.

With the CST simulation, we compare our analytical results with numerical results from CST for the cylindrical corrugated structure with  $q = 0.1$  and  $\hat{\omega}_c$ . As the result, we can observe a good matching in  $E_z$ - $z$  graph between analytical and numerical results fig.5.8 which is slightly better than the rectangular corrugated waveguide fig.3.4. In addition, we examine phase and group velocities and the CIP where the graph of phase and group velocities coincide. For the cylindrical corrugated waveguide, the CIP of analytical results is 384.46 GHz and 376.6 GHz when  $\hat{\omega}_c \approx 1.086$  for numerical results.

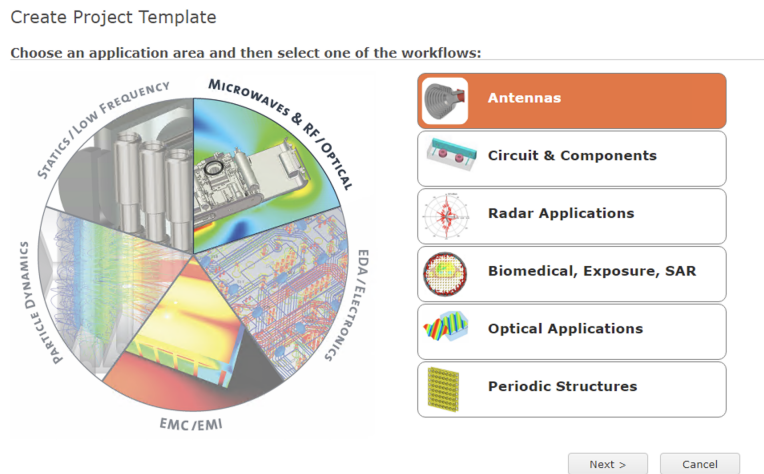
However, there are constraints that need to be considered. Firstly, a parameter  $q$  need to be small to get the good approximation, we found that by keeping  $q = 0.1$  (smooth corrugation) there will still be a good matching in graphs of analytical and numerical electric fields as shown in fig.5.15. For  $q = 0.1$ ,  $\hat{\omega}_c$  must be equal to 1.254 so there will be the CIP for this structure,  $\hat{k} = 2.857$ ,  $\beta_e = 0.53$  (92 KeV).

Another constraint for the good approximation is  $R'(z)$ ,  $R''(z)$  for the cylindrical corrugated waveguide and  $L'_x(z)$ ,  $L''_x(z)$  for rectangular corrugated waveguide have to be small values. The smaller  $R'$  and  $R''$  or  $L'_x(z)$  and  $L''_x(z)$ , the better of the approximation is. We represent this condition in  $\delta = \frac{R_0}{L_z}$  and  $\delta = \frac{L_0}{L_z}$ . Our mathematical model predicts that if  $\delta$  is small, the graph of analytical and numerical results will match. Nevertheless, the results do not follow the prediction as shown in fig.5.14. To improve an approximation and find out the reason of this, we will continue on this problem as future works.

# Appendix A

## Create a Structure

1. Create a new template → Choose Microwaves and RF/Optical Antennas → Select workflow Waveguide (Horn, Cone, etc.) → Click Next → Click Finish .



2. In Modeling → Click a drop-down of Curves → Select Analytic Curve to create the corrugated line.

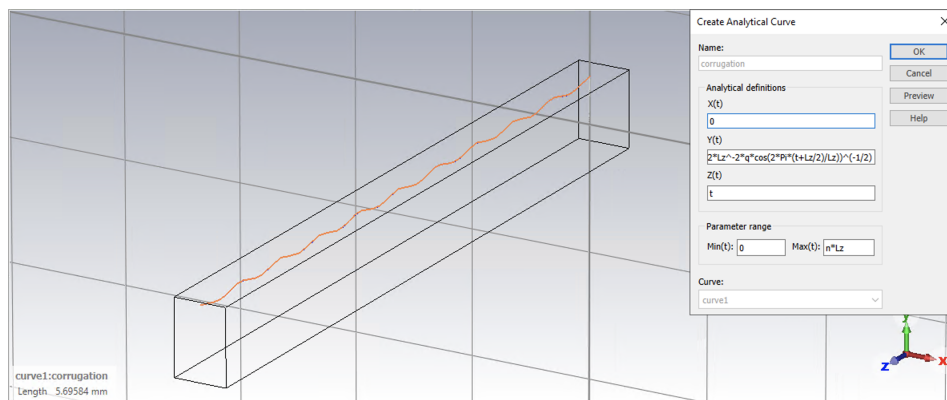


Figure A.1: Analytical definitions, we define  $X(t) = 0$ ,  $Y(t) = (R_0^{-2} + 2(\chi_0^1)^{-2}\pi^2L_z^{-2}q \cos(2\pi(t + L_z/2)/L_z))^{-\frac{1}{2}}$ , and  $Z(t) = t$ . The length of the structure spans from  $t = 0$  to  $t = n \cdot L_z$ , where  $n$  is periods of structure.

3. In Modeling → Click a drop-down of Curves → Select 3D Polygon to create a line at the beginning  $z = 0$ , the end  $z = n \cdot L_z$  and line at the center of the structure.

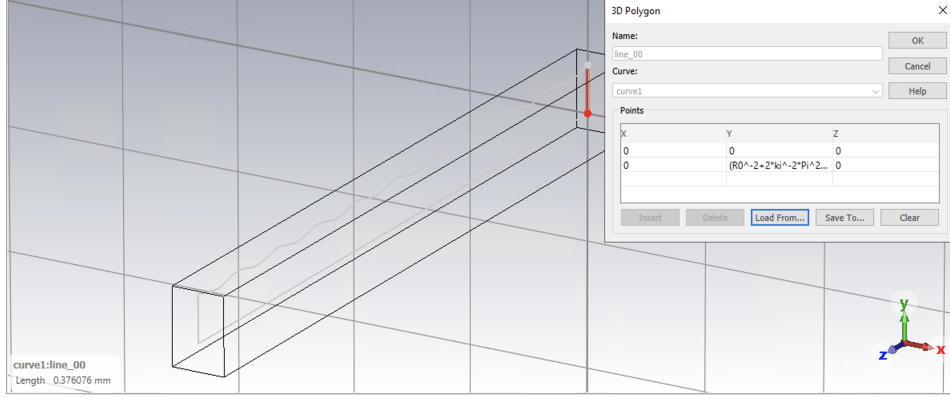


Figure A.2: Line at the beginning of the structure from a point  $(x_1 = 0, y_1 = 0, z_1 = 0)$  to a point  $(x_2 = 0, y_2 = (R_0^{-2} + 2(\chi_0^1)^{-2}\pi^2 L_z^{-2}q \cos(2\pi(0 + L_z/2)/L_z))^{-\frac{1}{2}}, z_2 = 0)$ .

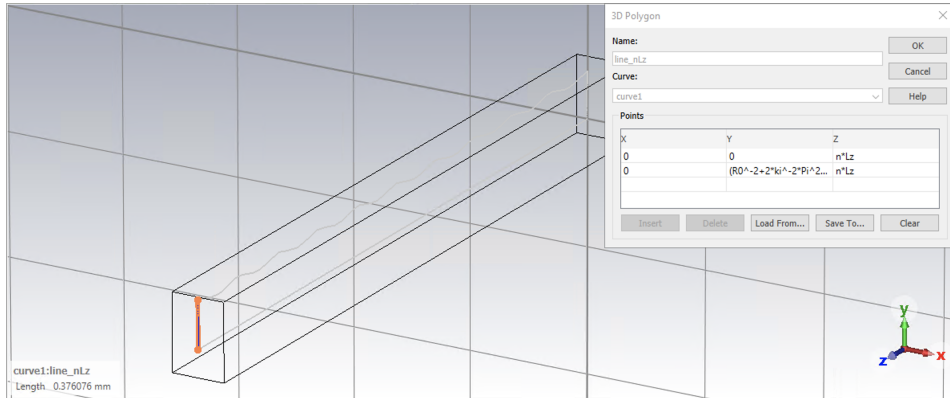


Figure A.3: Line at the end of the structure from a point  $(x_1 = 0, y_1 = 0, z_1 = n \cdot L_z)$  to a point  $(x_2 = 0, y_2 = (R_0^{-2} + 2(\chi_0^1)^{-2}\pi^2 L_z^{-2}q \cos(2\pi(n \cdot L_z + L_z/2)/L_z))^{-\frac{1}{2}}, z_2 = n \cdot L_z)$ .

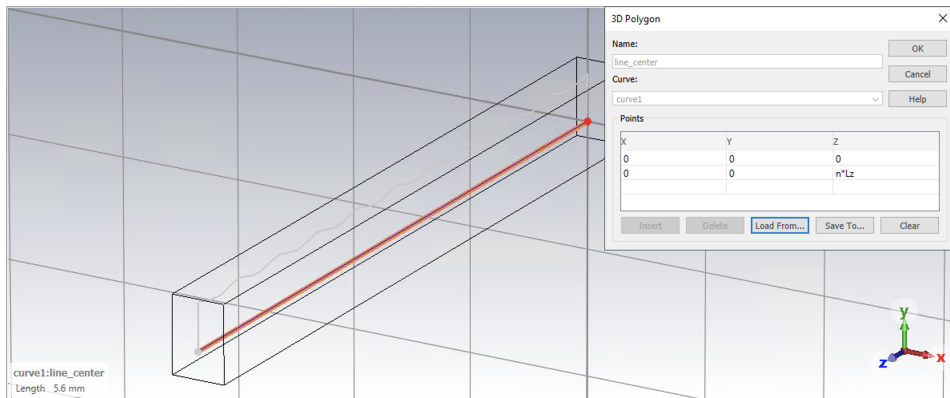


Figure A.4: Line at the center of the structure from a point  $(x_1 = 0, y_1 = 0, z_1 = 0)$  to a point  $(x_2 = 0, y_2 = 0, z_2 = n \cdot L_z)$ .

- In Modeling → Select Picks → Click at the lines that created in step 2 and step 3 → Click a drop-down of Extrude Curve → Select Cover Curve.

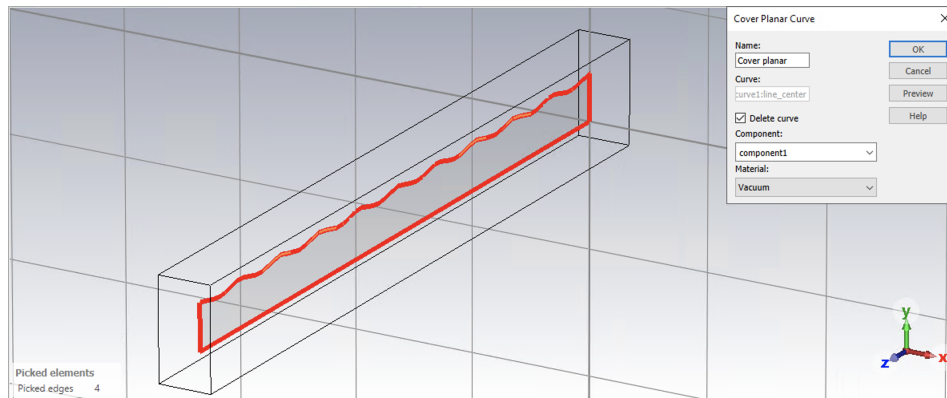


Figure A.5: In the Cover Planer Curve setup, choose Vacuum for being the Material of the planer.

- In Modeling → Click Rotate Face → Set up a rotated axis → set up a Rotate Face.

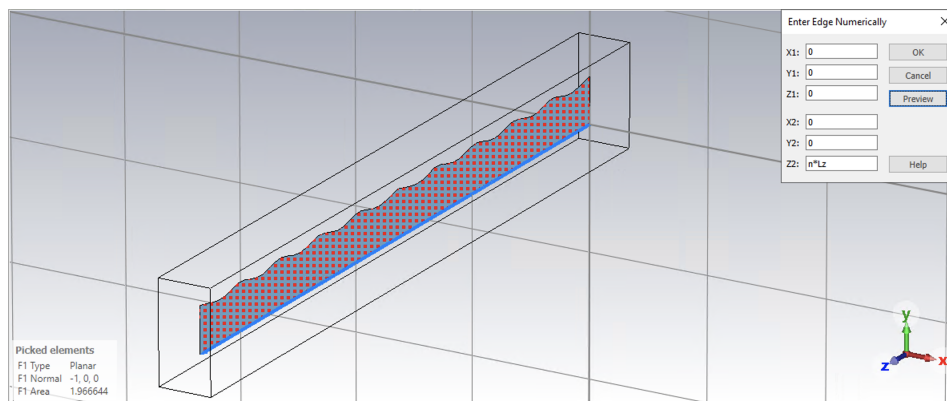


Figure A.6: Set up a rotated axis numerically, from a point  $(x_1 = 0, y_1 = 0, z = 0)$  to a point  $(x_2 = 0, y_2 = 0, z_2 = n \cdot L_z)$ .

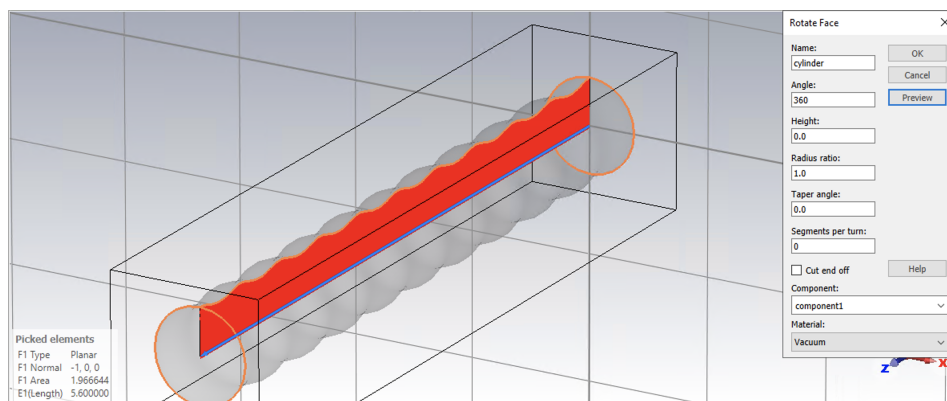


Figure A.7: Set up a Rotate Face, choose an Angle to be 360 (degree) and Material to be Vacuum.

---

After rotate a surface, the result is the vacuum cylindrical corrugated.

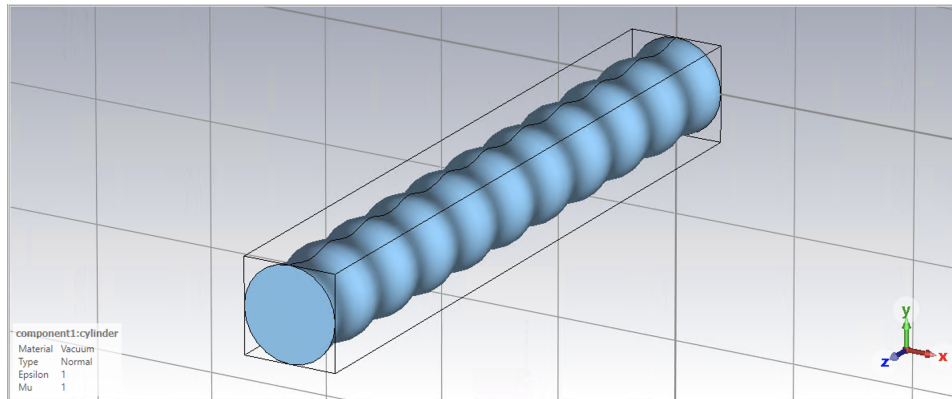


Figure A.8: The cylindrical corrugated waveguide which its material is vacuum. With parameters;  $q = 0.1$ ,  $R_0 = 0.35\text{mm}$ ,  $L_z = 0.56\text{mm}$ ,  $n = 10$  and  $\omega_c \approx 1.225$ .

# Bibliography

- [1] M. Tonouchi, “Cutting-edge thz technology,” *Nat. Photonics*, vol. 1, pp. 97–105, 02 2007.
- [2] P. Ashish, D. Sonawane, K. Erande, and D. Derle, “Terahertz technology and its applications,” *Drug Invention Today*, vol. 5, p. 157–163, 06 2013.
- [3] A. Fitzgerald, V. Wallace, M. Jimenez-Linan, L. Bobrow, J. Pye, A. Purushotham, and D. Arnone, “Terahertz pulsed imaging of human breast tumors 1,” *Radiology*, vol. 239, pp. 533–40, 06 2006.
- [4] R. Woodward, V. Wallace, D. Arnone, E. Linfield, and M. Pepper, “Terahertz pulsed imaging of skin cancer in the time and frequency domain,” *Journal of biological physics*, vol. 29, pp. 257–9, 06 2003.
- [5] J. Federici, B. Schulkin, F. Huang, D. Gary, R. Barat, F. Oliveira, and D. Zimdars, “Thz imaging and sensing for security applications - explosives, weapons and drugs,” *Semiconductor Science and Technology*, vol. 20, p. S266, 06 2005.
- [6] Y. Lu and X. Zheng, “6g: A survey on technologies, scenarios, challenges, and the related issues,” *Journal of Industrial Information Integration*, vol. 19, p. 100158, 07 2020.
- [7] J. Faist, F. Capasso, D. Sivco, C. Sirtori, A. Hutchinson, and A. Cho, “Quantum cascade laser,” *Science*, vol. 264, pp. 553–556, 04 1994.
- [8] D. Auston, K. Cheung, and P. Smith, “Picosecond photoconducting hertzian dipoles. appl. phys. lett. 45, 284-286,” *Applied Physics Letters*, vol. 45, pp. 284 – 286, 09 1984.
- [9] D. You, R. Jones, P. Bucksbaum, and D. Dykaar, “Generation of high-power sub-single-cycle 500-fs electromagnetic pulses,” *Optics letters*, vol. 18, p. 290, 02 1993.
- [10] Y. Zhang, K. Li, and H. Zhao, “Intense terahertz radiation: generation and application,” *Frontiers of Optoelectronics*, vol. 14, 12 2020.
- [11] J. H. Booske, R. J. Dobbs, C. D. Joye, C. L. Kory, G. R. Neil, G.-S. Park, J. Park, and R. J. Temkin, “Vacuum electronic high power terahertz sources,” *IEEE Transactions on Terahertz Science and Technology*, vol. 1, no. 1, pp. 54–75, 2011.

- [12] J. H. Booske, R. J. Dobbs, C. D. Joye, C. L. Kory, G. R. Neil, G.-S. Park, J. Park, and R. J. Temkin, "Vacuum electronic high power terahertz sources," *IEEE Transactions on Terahertz Science and Technology*, vol. 1, no. 1, pp. 54–75, 2011.
- [13] A. Fisher, Y. Park, M. Lenz, A. Ody, R. Agustsson, T. Hodgetts, A. Murokh, and P. Musumeci, "Single-pass high-efficiency terahertz free-electron laser," *Nature Photonics*, vol. 16, pp. 1–7, 06 2022.
- [14] R. Kompfner and N. T. Williams, "Backward-wave tubes," *Proceedings of the IRE*, vol. 41, no. 11, pp. 1602–1611, 1953.
- [15] J. R. Pierce, "Traveling-wave tubes," *The Bell System Technical Journal*, vol. 29, no. 2, pp. 189–250, 1950.
- [16] S. Siaber, J. Gratus, R. Seviour, S. Jamison, and T. Boyd, "Corrugated waveguide with matched phase and group velocities: an extended regime of wave-beam interaction," *Optics Express*, vol. 32, 06 2024.
- [17] X. Xu, Y. Wei, F. Shen, Z. Duan, Y. Gong, H. Yin, and W. Wang, "Sine waveguide for 0.22-thz traveling-wave tube," *IEEE Electron Device Letters*, vol. 32, no. 8, pp. 1152–1154, 2011.
- [18] S. Fang, J. Xu, X. Jiang, L. Xia, G. Wu, Q. Li, C. Ding, X. Yu, W. Wang, Y. Gong, and Y. Wei, "Study on w-band sheet-beam traveling-wave tube based on flat-roofed sine waveguide," *AIP Advances*, vol. 8, p. 055116, 05 2018.
- [19] L. Zhang, G. Ma, Y. Jiang, R. Song, W. Lei, W. Wei, P. Hu, H. Chen, and Y. Wei, "A wideband 220-ghz traveling wave tube based on slotted piecewise sine waveguide," *IEEE Electron Device Letters*, vol. 44, no. 8, pp. 1352–1355, 2023.
- [20] R. Ives, "Microfabrication of high-frequency vacuum electron devices," *Plasma Science, IEEE Transactions on*, vol. 32, pp. 1277 – 1291, 07 2004.
- [21] D. Gamzina, L. G. Himes, R. Barchfeld, Y. Zheng, B. K. Popovic, C. Paoloni, E. Choi, and N. C. Luhmann, "Nano-cnc machining of sub-thz vacuum electron devices," *IEEE Transactions on Electron Devices*, vol. 63, no. 10, pp. 4067–4073, 2016.
- [22] C. Cordeiro, A. Ng, and H. Ebendorff-Heidepriem, "Ultra-simplified single-step fabrication of microstructured optical fiber," *Scientific Reports*, vol. 10, p. 9678, 06 2020.
- [23] T. P. Wangler, *Periodic Accelerating Structures*, ch. 3, pp. 53–82. John Wiley & Sons, Ltd, 2008.
- [24] T. P. Wangler, *RF Acceleration in Linacs*, ch. 2, pp. 32–52. John Wiley & Sons, Ltd, 2008.